Geoderma 472 (2026) 117911

Contents lists available at ScienceDirect

Geoderma

journal homepage: www.elsevier.com/locate/geoderma

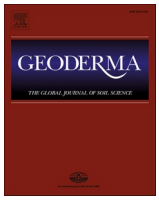

Connecting saturated hydraulic conductivity to soil aggregation on croplands along a European climate transect

D.J. Burger [a,*], W. Amelung [a,b], A.P. Heidtmann [a], M.S. Geske [a], H. Schimmel [a], M. Andersson [c], J. Cobos Sabate [d], R. Díaz Delgado [d], P. Gundersen [e], M. Ibañez [f], K.H. Jensen [g], M.C. Looms [g], P.E. Redondo-Hasselerharm [h], A. Rico [i], M.T. Sebastià [f,j], S. Spielvogel [k], L. Vesterdal [e], J. Wallsten [l], J. Westin [m], S. Zacharias [n], I. Zimmerman [k], L. Weihermüller [b], H. Vereecken [b], S.L. Bauke [a,o]

[a] Institute of Crop Science and Resource Conservation (INRES) – Soil Science and Soil Ecology, University of Bonn, Nussallee 13, 53115 Bonn, Germany
[b] Forschungszentrum Jülich GmbH, Institute of Bio- and Geosciences, IBG-3: Agrosphere, Wilhelm Johnen Str, 52425 Jülich, Germany
[c] Unit for Field based Forest Research, Asa Research Station, Swedish University of Agricultural Sciences, Lammhult, Sweden
[d] Estación Biológica de Doñana, EBD-CSIC, Calle Americo Vespucio, 26, Isla de la Cartuja, Sevilla 41092, Andalusia, Spain
[e] Department of Geosciences and Natural Resource Management, University of Copenhagen, 1958 Frederiksberg C, Denmark
[f] Laboratory of Functional Ecology and Global Change (ECOFUN), Forest Science and Technology Centre of Catalonia (CTFC), Solsona, Spain
[g] Department of Geosciences and Natural Resource Management, University of Copenhagen, Øster Voldgade 10, Copenhagen 1350, Denmark
[h] IMDEA Water Institute, Avda. Punto Com 2, 28805 Alcalá de Henares, Madrid, Spain
[i] Cavanilles Institute of Biodiversity and Evolutionary Biology, University of Valencia, C/Catedrático José Beltrán 2, Valencia, Paterna E-46980, Spain
[j] Group GAMES and Department of Agricultural and Forest Sciences and Engineering, School of Agrifood and Forestry Engineering and Veterinary Medicine, University of Lleida, Lleida, Spain
[k] Institute of Plant Nutrition and Soil Science, Christian-Albrechts-University, Hermann-Rodewald-Str. 2, 24118 Kiel, Germany
[l] Department of Crop Production Ecology, Swedish University of Agricultural Sciences, 901 83 Umeå, Sweden
[m] Unit for Field-Based Forest Research, Swedish University of Agricultural Sciences, SE-922 91 Vindeln, Sweden
[n] Helmholtz Centre for Environmental Research GmbH - UFZ, Permoserstr. 15, 04318 Leipzig, Germany
[o] Soil Sciences, Faculty of Agriculture, Civil and Environmental Engineering, University of Rostock, Justus von Liebig Weg 6, 18059 Rostock, Germany

ARTICLE INFO

Handling Editor: Dr. H Neely

Keywords:
Hydraulic conductivity
Soil structure
Climatic gradient
Soil aggregates
Pedotransfer functions

ABSTRACT

Soil aggregates facilitate the infiltration of water into soils. However, information on soil aggregates has not been used for prediction of saturated hydraulic conductivity (*Ks*) in hydrological or Land Surface Models (LSM) so far. We hypothesized that aggregate size, described by the mean weight diameter (MWD), is a key driver of *Ks* across different climates. To test this, 49 cropland soils were sampled along a climosequence from Northern Sweden to Southern Spain. Tension infiltrometer measurements were performed to determine *Ks*, which were then predicted using basic soil properties and aggregate size. 10 existing pedotransfer functions (PTFs) using easy-to-measure soil properties were tested. Without recalibration of the regression coefficients to our data, all existing PTFs performed poorly. After calibration, Root Mean Squared Error (RMSE) and R^2 values improved to 0.81–1.10 (ln*Ks*) and 0.10–0.51, respectively. Subsequently, two new regression-based PTFs were developed, using soil organic carbon (SOC) content and soil texture as predictors, and explained up to 61% of the data variability. Additionally, MWD could be predicted using soil texture, bulk density, and SOC, with an R^2 of 0.9 and an RMSE of 343 μm, which allowed replacement of laboratory MWD measurements. Aggregate MWD alone could not predict *Ks*, but the performance of the two newly developed PTF substantially reduced the RMSE and increased the R^2 up to 0.68 after combining MWD with soil texture and SOC. Using simple linear models for predicting aggregate MWD and implementing MWD into PTFs allows for better *Ks* estimation, and thus, water infiltration and transport in soils.

* Corresponding author.
E-mail address: dburger@uni-bonn.de (D.J. Burger).

https://doi.org/10.1016/j.geoderma.2026.117911
Received 6 November 2025; Received in revised form 29 May 2026; Accepted 18 June 2026
Available online 23 June 2026

1. Introduction

Soils link atmospheric and hydrological processes with the biosphere (Fatichi et al., 2020) and thus play an important role in regulating the water cycle. The ability of soils to facilitate water infiltration and transmit water is described by the functions of water retention and hydraulic conductivity (Caplan et al., 2019). Additionally, saturated hydraulic conductivity (*Ks)* is a key parameter in hydrological or land surface models (LSMs) to describe the partitioning of water at the soil surface into runoff and infiltration (Gutmann and Small, 2007; Vereecken et al., 2019). *Ks* measurements are time consuming and sample collection in large regions is not feasible. Therefore, LSMs use pedotransfer functions (PTFs) to predict *Ks* from soil data that is more easily obtainable, such as soil texture, bulk density, and soil organic carbon (SOC) content (Vereecken et al., 2022).

However, most PTFs do not account for soil structure, and thus the impact of soil structure on *Ks*, such as fast infiltration of water into larger inter-aggregate pores, will not be predicted. Hence, traditional PTFs that do not allow soil structural information as predictors may underestimate *Ks*, leading to false estimates of other parts of the water cycle (Levin et al., 2023; Zhang and Schaap, 2019), such as an overestimation of runoff and an underestimation of infiltration (Fatichi et al., 2020). Including soil structure into PTFs to estimate *Ks* more precisely, could thus lead to an improved description of infiltration in LSMs (van Looy et al., 2017).

Soil structure, i.e., the arrangement of soil particles and aggregates leading to different pore spaces, can be described using the solid phase perspective, focusing on soil aggregates, or the pore space perspective (Rabot et al., 2018). The pore space perspective is often used in relation to soil hydraulic properties (Vogel et al., 2022), and distinguishes macropores from meso- and micropores by their functionality, as they are more subject to gravitational drainage, and therefore, only contain water at or close to saturation (Jarvis, 2007). Soil porosity and structure can be directly measured using imaging techniques, mercury porosimetry, or gas adsorption, and can be indirectly derived from soil water retention curves (Diaz-Zorita et al., 2002). Even though imaging techniques have been made available for many scientific disciplines, it is still a time and cost intensive process and only small sample volumes can be measured (Rabot et al., 2018).

A quicker and more cost effective way of measuring soil structure is focusing on the soil aggregates, which is often done by aggregate fractionation (Diaz-Zorita et al., 2002; Rabot et al., 2018; Vogel et al., 2022). The amount of macro- (diameter $>$ 250 μm) and microaggregates (diameter $<$ 250 μm) strongly influences the pore size distribution (Vogel et al., 2022) and aggregates can therefore function as a surrogate to describe a more complex soil structure (Garland et al., 2024; Koestel et al., 2021; Six et al., 2004). In order to provide a single parameter of soil structure, the size and amount of micro- and macroaggregates are usually summarised as the mean weighted diameter (MWD) (Pulido Moncada et al., 2015).

Nevertheless, aggregate size fractionation to determine the MWD using sieving methods remains laborious and time-consuming. Hence, some studies have used surrogates for soil structure that are easier to obtain, such as gravel content and the presence of a mattic epipedon, a surface layer of intertwined grass roots that is common in alpine environments, e.g. at the Qinghai-Tibetan plateau (Wang et al., 2024), chemical properties like cation exchange capacity (CEC) or pH (Tóth et al., 2015), or the MWD itself is estimated by PTF (Purushothaman et al., 2022). Still, data on aggregate MWD across different land uses or climatic conditions are scarce, and the specific effect of soil aggregates on *Ks* therefore remains largely unknown.

This study aims at improving predictions of *Ks* by incorporating information on aggregate size, specifically the aggregate MWD, as a surrogate of soil structure into newly developed PTFs. We compare these newly developed PTFs to eight existing, commonly used PTFs that have been validated in literature and are based on regression analysis as given in the reviews of Zhang and Schaap (2019) and three PTFs that include the aggregate MWD, developed by Basset et al. (2023). In order to use them outside the spatial context that they were developed for, these PTFs were all recalibrated to our data as suggested by (Arbor et al., 2023). We hypothesized (1) that the recalibration of the existing PTFs to our dataset will lead to higher predictive power for *Ks* (larger R^2 and lower RMSE) compared to uncalibrated (standard) PTFs, and (2) that including the soil aggregate MWD leads to better predictions of *Ks* than only including soil texture and SOC. We assumed also that (3) aggregate size can be predicted from basic soil properties, such as soil texture or soil group according to the World Reference Base (WRB (IUSS, 2022)), but that PTF performance decreases when using predicted instead of measured aggregate MWD. To test these hypotheses, we conducted infiltration experiments in different croplands across Europe to determine field measured *Ks*. We then related *Ks* to aggregate MWD, basic soil properties, and the field conditions soil water content and soil temperature as indirect climatic indicators to be able to compare the sites along the European climate gradient.

2. Methods

2.1. Description of the study area

Soil samples were taken in 13 sites, distributed on a transect from Northern Sweden to Southern Spain (Fig. 1). On this transect, the mean annual temperature (MAT) of the sites ranged from 1.6 to 16.1°C and mean annual precipitation (MAP) ranged from 463 to 1053 mm. The soils sampled were characterized as Cambisols, Regosols, Luvisols, Gleysols, Fluvisols, Podzols, Arenosols, and Chernozems according to WRB (IUSS, 2022) and information on the basic soil properties are listed in the Supplementary Materials Tables S1 and S2 as well as in Fig. S1. Clay content was always below 33% and each sampling site was regularly tilled for more than 10 years.

2.2. Sampling design

Each site was sampled with at least two independent field replicates, with two pseudo replicate samples taken in approx. 5 m distance from

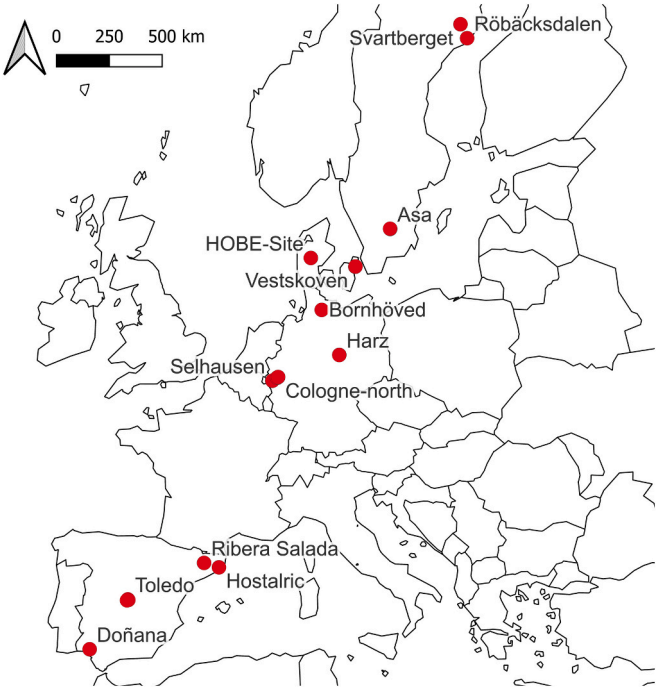

Fig. 1. Overview of the sampling sites along the North-South climosequence.

each other in each field replicate (Fig. 2). Exceptions are described in Table S1. In total, 13 sites were sampled, of which all had three field replicates, except from the Asa, Cologne-North, and Doñana site, which had four, 16 divided across three texture groups, and two field replicates respectively. This resulted in 52 croplands sampled and measured. The results of the pseudo replicates at each field site (Fig. 2), were averaged and field replicates per sampling location on the transect were weighted equally. Soil samples were taken at 0–10 cm depth by cutting out a block of about 10 x 10 x 20 cm (w x d x l) with a spade. From this block, a subsample was cut and kept undisturbed for soil aggregate fractionation, while the remaining soil was air-dried, homogenized, and stored for texture and SOC analysis. Additionally, an undisturbed sample was taken using Kopecky rings (100 cm^3) for bulk density and volumetric soil water content determination.

Infiltration rates were measured with a hood infiltrometer (UGT GmbH, Müncheberg, Germany), which is a variation of a tension infiltrometer with an effective hood radius of 8.8 cm as described in detail by Schwärzel and Punzel (2007). At each site, the litter layer including harvest residues, if present, was removed and vegetation was trimmed to 0.5 cm above the soil surface prior to infiltration measurements. Before the measurement started, the initial volumetric soil water content and soil temperature were measured in the first 7.5 cm of the soil with a Fieldscout TDR 150 system (Spectrum Technologies, Inc, Aurora, United States). These measurements were done approximately 50 cm away from the spot where the infiltration measurement was conducted. Infiltration measurements were performed at a tension of 0 and −2 cm for saturation and near-saturation, respectively, until steady state flow occurred.

2.3. Calculation of the soil hydraulic conductivity

Before calculating the hydraulic conductivity, all infiltration measurements were inspected. Measurements at three out of 52 sites were marked as outliers due to problems with data logging. These sites were excluded from the dataset and all PTF development and analyses were conducted with those 49 sites. The measured steady state infiltration rates were used to calculate the saturated hydraulic conductivity. Measurements at two tensions were required to account for the 3D flow of water in the soil. Data were analysed using the models of Gardner (1958) and Wooding (1968) (Eqs. (1) and (2)). The steady state infiltration rate Q was corrected for the cross-sectional area of the hood by multiplying the measured infiltration rate by 0.313. Subsequently, the Gardner coefficient α (cm^{-1}), which is the slope of the measured infiltration curve, was calculated from the steady-state infiltration rates Q_1 and Q_2 (mm min^{-1}) measured at the two tensions $h_1 = 0$ cm and $h_2 = -2$ cm:

$$\alpha = \frac{\ln\left(\frac{Q_1}{Q_2}\right)}{(h_1 - h_2)} \quad (1)$$

In a next step, the Wooding (1968) equation was used to calculate the hydraulic conductivity (K) at tension i based on the calculated Gardner coefficient and measured steady state infiltration rate.

$$K(h_i) = \frac{\frac{Q_i}{\pi^* a^2}}{\left(1 + \frac{4}{\pi^* a^2}\right)} \quad (2)$$

Here, it should be noted, that we only used infiltration rates measured at $h = -2$ cm to estimate the Gardner coefficient, but we did not further calculate and analyse K at $h = -2$ cm in the context of this study.

2.4. Laboratory analysis

2.4.1. Basic laboratory analyses

The volumetric water content and dry matter bulk density of the 100 cm^3 undisturbed samples in the Kopecky rings were determined by drying the samples at 105 °C for 48 h. The disturbed soil samples were dried at 40 °C and an aliquot of 10 g was taken for hydrophobicity analysis. Hydrophobicity was determined by the water droplet penetration time (WDPT) test according to Doerr (1998). The bulk soil samples were sieved at 2 mm and used for texture analysis by the combined sieve and pipette method (ISO 11277, 2002) in duplicate. Here, it has to be noted, that the sand fraction was 2000 to 63 µm according to the German soil texture classification (DIN ISO 11277). Another aliquot of the dried and sieved sample was milled and analysed for total carbon content by elemental analysis (vario EL cube; Elementar, Hanau, Germany). For samples with pH < 6.0 total carbon content was assumed to represent SOC content. Samples with pH > 6.0 were additionally analysed by dry combustion using a temperature ramp to separate organic carbon (released below 600 °C) and inorganic carbon (released above 600 °C) (soliTOC Cube; Elementar, Hanau, Germany).

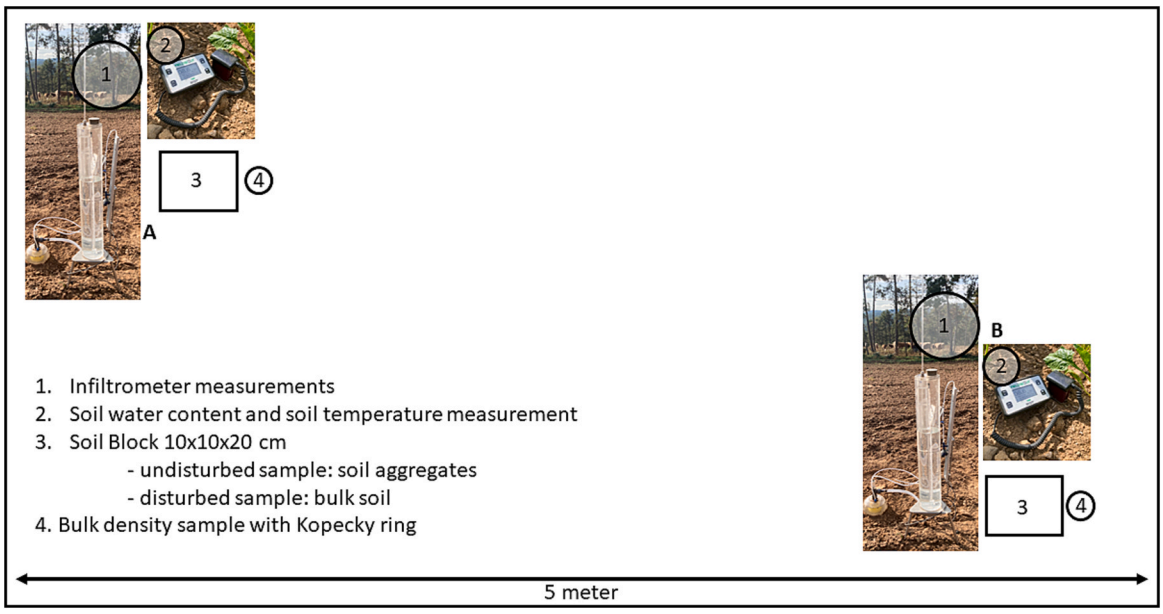

Fig. 2. Overview of a field replicate of a sampling site, showing the measurements and samples (1–4) that were taken at the pseudo replicates (A and B).

2.4.2. Aggregate size fractionation

Aggregate size fractionation was carried out by wet sieving as described by Lobe et al. (2011). In brief, 20 g of the undisturbed sample was slowly wetted for five minutes on a glass fibre filter placed on the top sieve of a sieving tower submerged in distilled water. Samples with extreme hydrophobicity (WDPT > 10 min) received a pre-treatment with a water/ethanol solution (24 vol%) solution. According to Doerr (1998), the water droplet penetration time of >10 min (class 3, severely water repellent) corresponds to direct droplet penetration of a water/ethanol solution with a concentration of 24 vol%. Therefore, the hydrophobic samples were placed on a glass fibre filter held by a sieve and put in a beaker filled with 100 ml water/ethanol solution (24 vol%). The samples were slowly wetted for 5 min with the ethanol solution similar to those samples that were wetted with distilled water. After pre-wetting, the samples were wet sieved on a sieve tower with sieves of 2800, 2000, 500, 250, and 53 μm mesh size (Retsch®, Haan, Germany), respectively. The sieve tower was moved 3 cm up and down in a bucket with distilled water for 2 min at an oscillation speed of 30 rounds per minute. Finally, the sieved fractions were collected from the sieves by rinsing the material into a glass beaker. The samples were dried at 40 °C and the corresponding aggregate weight was determined. The smallest fraction (<53 μm) was left to settle overnight in the bucket after a few drops of $MgCl_2$ were added. Thereafter, the supernatant was removed using a jet pump. The settled material was rinsed into a centrifuge cup and was centrifuged for 20 min at a speed of 1815×*g*. The supernatant was then discarded, the pellet containing the <53 μm aggregate fraction was dried at 40 °C and subsequently weighed.

2.4.3. Calculation of the MWD of the soil aggregates

The weight of the individual soil aggregate fractions was corrected for the sand fraction derived from the bulk soil texture analysis. Sand correction of the aggregate fractions was conducted following the recommendations by Six et al. (1998). The >2.8 mm, 2.8–2 mm, and 2000–500 μm aggregate fractions were corrected for all three sand fractions, and the 500–250 and 250–53 μm aggregate fractions were corrected for the medium (630–200 μm) and fine sand (200–63 μm) fraction. The smallest aggregate fraction of <53 μm was not corrected for sand content.

The mean weight diameter (MWD) of the soil aggregates was calculated according to van Bavel (1950) modified by Kemper and Rosenau (1986).

2.5. Pedotransfer function development

Eight existing PTFs based on regression models were derived from the review of Zhang and Schaap (2019), which reviewed the most commonly used PTFs. All of these PTFs have been validated in literature (Wang et al., 2012; Weynants et al., 2009). The PTF by Wösten et al. (1999) is based on the European HYPRES database, and therefore, covers the pedoclimatic conditions sampled in our study. The main criteria for PTF selection in this study was that the PTF was developed using linear regression, and that the soil properties used in the PTF were also available in our database, e.g. soil texture, SOC, and bulk density, which excluded the regression-based PTFs of Ahuja et al. (1989) and Tóth et al. (2015). Three additional PTFs that included soil aggregation to estimate *Ks*, developed by Basset et al. (2023), were tested as well (Tables 1 and S3). To date these are the only existing PTFs for *Ks* that use aggregate MWD as a predictor and are have been also developed using regression. Some of the original (uncalibrated) PTFs, i.e., the Cosby 1, Cosby 2, Wang, and Basset PTFs, predicted *Ks* in other units than cm day^{-1} or used no or other transformations as we did for our data. These PTFs were edited to ensure that they estimated *Ks* in cm day^{-1} and that the *Ks* was log transformed using a natural logarithm. Here, it has to be noted, that the transformation to the same *Ks* units also adjusted the regression coefficients, however they were not recalibrated to our data.

Some of the PTFs required several further adjustments of the data.

Table 1
Overview of the pedotransfer functions (PTFs) used. PTFs in italics include soil aggregation as predictor.

PTF name	Database region	Number of samples	Predictors	Type of *Ks* measurement
Cosby 1/ Cosby et al. (1984)	United States	1448	Sand	Laboratory
Cosby 2/ Cosby et al. (1984)	United States	1448	Sand, clay	Laboratory
Vereecken 1/ Vereecken et al. (1990)	Belgium	127	Sand, clay, SOM, BD	Laboratory
Vereecken 2/ Vereecken et al. (1990)	Belgium	127	Texture principal components, SOM, BD	Laboratory
Wösten/ Wösten et al. (1999)	HYPRES (Europe)	1139	Silt, clay, BD, SOM	Various methods, field and laboratory
Li/Li et al. (2007)	Fengqui, China	36	Sand, silt, clay, SOM	Laboratory
Weynants/ Weynants et al. (2009)	Belgium (Vereecken database)	136	Sand, BD, SOC	Laboratory
Wang/Wang et al. (2012)	Loess plateau, China	382	Silt, sand, SOC, BD, elevation	Laboratory
Basset 1/ Basset et al. (2023)	*Global meta-analysis*	*112*	*MWD*	*Laboratory and field*
Basset 2/ Basset et al. (2023)	*Global meta-analysis*	*82*	*MWD, SOC*	*Laboratory and field*
Basset 3/ Basset et al. (2023)	*Global meta-analysis*	*64*	*MWD, SOC, BD*	*Laboratory and field*
PTFs developed on our dataset				
PTF A	European climosequence	49	Sand, clay SOC	Field, Hood infiltrometer
PTF B	*European climosequence*	*49*	*MWD, clay, SOC*	*Field, Hood infiltrometer*
PTF C	European climosequence	49	Sand, clay, SOC, soil water content, soil temperature	Field, Hood infiltrometer
PTF D	*European climosequence*	*49*	*MWD, clay, SOC, soil water content, soil temperature*	*Field, Hood infiltrometer*

BD is bulk density (g cm^{-3}), MWD is mean weight diameter of the aggregates, SOC is soil organic carbon (%), Ks is the saturated hydraulic conductivity.

Whenever soil organic matter (SOM) was used in the PTF instead of the measured SOC, the SOC content was divided by 0.6 to obtain SOM. For the Vereecken 2 PTF the soil texture predictors were transformed to principal components to reduce dimensionality (Vereecken et al., 1990) using the package factoextra (R Core Team, 2025) in R (version 4.5.1). In order to adjust this for our texture classes, a principal component analysis was carried out on our data using the following soil texture classes: coarse sand (2000 μm-630 μm), medium sand (630–200 μm), fine sand (200–63 μm), coarse silt (63–20 μm), medium silt (20–6.3 μm), fine silt (6.3–2 μm), and clay (<2 μm), as well as the geometrical mean

particle size (GMPS) and geometrical standard deviation (GSD) according to Shirazi and Boersma (1984). Five principal components (PCs) were chosen that had similar Eigenvectors of the texture classes and GMPS and GSD, to ensure that the principal components reflect similar information. The results of the principal component analysis and comparison to the principal components in the Vereecken 2 PTF is explained in Section 3.1.1. The Weynants PTF was developed to predict K^*, which is supposed to act as a "matching point" of K at a pressure head of $h = 0$ to overcome problems of strong bimodality, especially in the hydraulic conductivity characteristics. Therefore K^* can be slightly to substantially lower than Ks (Weynants et al., 2009). Irrespective of this constraint, the Weynants PTF was used to predict field measured Ks in this study. All PTFs and their predictors as included in this study are described in Table S3.

As a second step, the regression coefficients of the existing PTFs were calibrated by refitting the PTF to our data. Such recalibration might be necessary since measurement locations as well as the type of infiltration measurement used to build the PTFs differ from those in our study and most PTFs were developed with texture data where sand was defined as the size fraction between 2000 and 50 μm.

Additionally, using the data on soil texture, SOC, MWD, initial soil water content, and soil temperature collected in this study, four new multiple linear regression PTFs (in the following denoted as PTF A to D) were developed to predict Ks (Table S3). In these new PTFs, the combination of initial soil water content and soil temperature was used as an indirect climate indicator instead of other climate descriptors like MAT or MAP. We opted for the soil water content and soil temperature to be able to describe the climatic conditions in the field that might influence the infiltration measurements in that moment and to be able to compare measurements along the climate transect. Also, most of the measurement and the sampling campaign was conducted in summer, and therefore, annual averages do not reflect the conditions during the measurements. The normality and homoscedasticity of the regression residuals were inspected and Ks, SOC, and volumetric soil water contents were log-transformed using a natural logarithm (ln transform). Predictors had to be at least slightly significant ($p < 0.1$) and stable at a 90% confidence level after bootstrap resampling with 500 repetitions to be included in the new PTF. Correlation between single predictors was not allowed to be higher than Pearson r of 0.8 or lower than −0.8. The predictors finally included in the recalibrated and newly developed PTF are described in detail in Tables 1, S3, and S4.

Lab procedures to obtain the aggregate MWD as required in some of our newly developed PTFs are time-consuming; we therefore additionally tested whether that information can be estimated from other easily available soil parameters. Thus, we compared four PTFs (MWD_PTF 1 to 4) to estimate the MWD using combinations of soil texture, bulk density, SOC soil water content and WRB soil group classification data (Supplementary Materials Table S4). PTF quality for MWD_PTF 1–4 was evaluated in the same way as those developed for Ks.

To test the applicability of the MWD_PTFs, we reanalysed the K_s PTFs that included the aggregate MWD as a predictor, i.e., the new PTFs B and D and the ones reported by Basset et al. (2023). For these PTFs we compared K_s estimated obtained by using the measured MWD and by using the estimated MWD derived from the four MWD_PTFs (Tables S3 and S4). In case of the Basset PTFs, this test was performed for both the calibrated (using our measured data) and uncalibrated PTFs.

2.6. Statistical analyses

Statistical analyses were conducted in R (version 4.5.1) using the packages agricolae, car, caret, corrplot, cowplot, dplyr, factoextra, ggplot2, ggsoiltexture, gridextra, lmtest, MASS, Metrics, purr, readxl, tidyr, and yardstick (R Core Team, 2025).

The predictive performance of all existing PTFs and the four new PTFs (A, B, C, and D) for the estimation of measured Ks was assessed by calculating their Akaike Information Criterion (AIC), Bayesian information criterion (BIC) and also their root mean squared error (RMSE).

In order to evaluate the PTF performance on unseen data, the RMSE and R^2 after 10-fold cross validation with 100 repetitions was calculated. Here, a correlation (cor) based R^2 was calculated according to Eq. (3), to ensure stability over the different folds.

$$R^2 = (cor(y, \hat{y}))^2 \quad (3)$$

For the newly developed PTFs, the PTF with the highest R^2, lowest RMSE, and stable regression coefficients ($p < 0.1$) after bootstrap resampling was considered as the best PTF. In addition, the best PTF had to show the lowest signs of overfitting, which was derived from the difference in RMSE and R^2 after the 10-fold cross validation with 100 repetitions, compared to the RMSE and R^2 of the PTF that was trained on the whole dataset.

3. Results

3.1. Predictions of the saturated hydraulic conductivity using existing and newly developed PTFs

3.1.1. Particle size classes of soil texture transformed to principal components

To include the particle size distribution according to the German classification system into the Vereecken 2 PTF, particle size classes were transformed to principal components, shown in Table 2. In the original Vereecken 2 PTF, the first, second, third, fifth, and sixth principal components (PCs) are used as predictors (Vereecken et al., 1990). In our dataset, the first PC of the Vereecken 2 PTF corresponded to our first PC. The other PCs in our data had slightly different Eigenvectors than those of the Vereecken dataset, but still represented similar variance in the texture data. In the Vereecken 2 PTF, PC2 corresponded to PC5 in our dataset, PC3 to our PC2, PC5 to our PC6, and PC6 to our PC3. In our dataset, PC1 reflected coarse texture in comparison to fine texture, PC2 reflected bimodality in the particle-size distribution, PC3 reflected the fine sand fraction, PC5 the clay content in comparison to coarse sand, and PC6 clay content and bimodality in the particle size distribution. These principal components explained 91.1% of the variation in our texture data (Table 2).

3.1.2. Performance of non-calibrated PTFs

Without calibration, i.e., without further adjustment of the regression coefficients to our dataset, all 11 existing PTFs performed poorly, exhibiting low correlation based R^2 values (0.001–0.28) and RMSE values of 1.9 to 11.1 (cm day^{-1} ln transformed Ks) (Fig. 3, Table 3). The range of Ks values predicted by the PTFs was small, for example, 3.4 to 60.9 cm day^{-1} using the Weynants PTF. Similar results in prediction accuracy were found for the Basset 1, Cosby 1, Cosby 2, and the Wang PTFs. On the other hand, the predicted Ks was sometimes extremely large, for example up to unrealistic 699,357,420 cm day^{-1} in the Li PTF for a site with high SOM content (9.8%). Other PTFs with a large range in predicted Ks values were the Vereecken 1 and Basset 2 PTF. Yet, the values predicted by these two PTFs were closer to the observed Ks measured by the hood infiltrometer (Table 3).

It is noteworthy that almost all PTFs that did not consider soil structural information predicted high Ks values where our measured values were low. On the other hand, they also predicted low Ks values where high Ks values had been measured, resulting in a negative regression slope between predicted and measured Ks (Fig. 3, Table 3). The PTFs that include soil structural information as inputs showed a positive slope of the regression, but still failed to predict the Ks values precisely (RMSE = 3.11–3.94, ln(Ks)). The only PTF that did not include soil structure and that did not show this pattern was the Vereecken 2 PTF, which included the principal components derived from our dataset as texture predictors (Table 2, Table 3).

Table 2
Mean and standard deviations of the texture fractions, geometric mean particle size (GMPS) and geometric standard deviation (GSD), as well as their values in each of the principal components, and principal component eigenvectors and the variance explained, similarly done as the Vereecken level 2 pedotransfer function (PTF) (Vereecken et al., 1990), but for our data.

Variable	Mean	Standard deviation	PC1	PC2	PC3	PC4	PC5	PC6	PC7	PC8	PC9
Coarse sand [%]	5.99	7.82	−0.294	0.241	0.490	−0.025	−0.637	−0.228	0.0424	0.290	−0.265
Medium sand [%]	22.21	19.47	−0.441	−0.057	−0.015	−0.192	0.412	0.334	−0.110	0.189	−0.660
Fine sand [%]	18.23	9.70	−0.128	0.212	−0.773	0.286	−0.288	−0.242	−0.007	−0.099	−0.328
Coarse silt [%]	18.91	13.96	0.342	−0.405	0.204	0.374	−0.110	0.121	0.463	−0.273	−0.470
Medium silt [%]	13.39	7.72	0.429	−0.167	0.020	−0.212	−0.281	0.086	−0.750	−0.159	−0.263
Fine silt [%]	6.69	4.72	0.315	0.241	−0.165	−0.762	−0.093	0.009	0.443	−0.072	−0.155
Clay [%]	14.60	7.89	0.325	0.379	0.217	0.136	0.490	−0.603	−0.096	0.029	−0.268
GMPS [μm]	74.13	82.07	−0.443	−0.157	0.141	−0.224	0.031	−0.345	−0.042	−0.766	0.004
GSD	7.09	2.42	0.021	0.689	0.160	0.215	−0.017	0.523	−0.043	−0.421	0.001
Eigenvalue			2.100	1.358	1.109	0.823	0.710	0.462	0.338	0.087	0.006
Variance explained [%]			49.01	20.48	13.66	7.52	5.60	2.37	1.27	0.08	0.00004

Coarse sand: 2000–630 μm, medium sand: 630–200 μm, fine sand: 200–63 μm, coarse silt: 63–20 μm, medium silt: 20–6.3 μm, fine silt: 6.3–2 μm, clay: <2 μm.

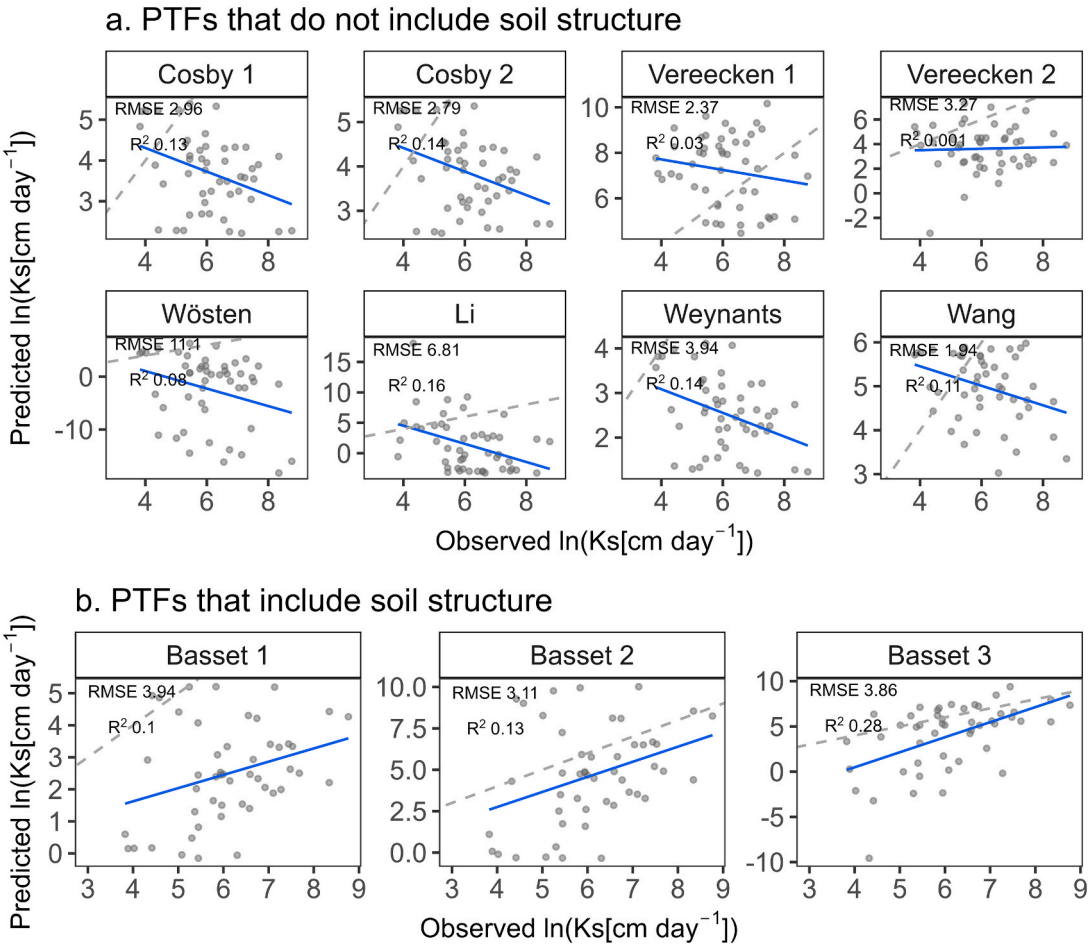

Fig. 3. Predictions of the saturated hydraulic conductivity (Ks), compared to the observed Ks values; using the original pedotransfer functions (PTFs). The first two rows depict PTFs which do not include structure (a) and the bottom row those PTFs which do include soil structure (b). RMSE Root Mean Squared Error (ln(Ks)), Ks = saturated hydraulic conductivity in cm day^{-1}, the R^2 value is correlation based. Blue lines display the regression line, whereas the grey dashed line displays the 1:1 line.

3.1.3. Effects of calibrating the regression coefficients of existing PTFs

In three of the eight PTFs that did not include soil structure, the coefficient of the sand content changed from positive to negative or negative to positive after calibration to our field measured *Ks* values compared to the laboratory measured *Ks* values that they were developed for (Table S5a), but this was not the case for the Vereecken 1 PTF and those of Wang and Li, where it did not change direction. Whenever the sand coefficient changed direction, it changed from positive to negative (Table S5a). In the Cosby 1, Cosby 2, and the Weynants PTFs the sand content term was significant or close to significant ($p < 0.1$ and $p < 0.05$). In the other PTFs, sand was not a significant predictor. The calibrated SOC terms were significant in the Vereecken 2 and Weynants PTF ($p < 0.001$ and $p < 0.01$, respectively), but not in the other PTFs.

After calibration, several coefficients changed by 1–2 orders of magnitude, for example, that for bulk density in the Vereecken 1, Vereecken 2, and Weynants PTFs or for the silt content in the Wang PTF. Some of the non-linear coefficients in Wösten's PTF changed up to 4 orders in magnitude, and some changed from positive to negative or vice

Table 3
PTF performance metrics of non calibrated PTFs, compared to the observed data, CV: cross validated model metric using 10-fold cross validation with 100 repetitions. R^2 = Coefficient of determination, correlation based, RMSE = Root Mean Squared Error (ln(Ks)), Ks = saturated hydraulic conductivity in cm day^{-1}, sd = standard deviation.

PTF	CV.R^2		CV RMSE		Minimum		Maximum	
	Mean	sd	Mean	sd	ln(*Ks*)	*Ks*	ln(*Ks*)	*Ks*
Basset 1	0.34	0.30	3.91	0.54	−0.15	0.86	5.20	182
Basset 2	0.35	0.30	3.03	0.72	−0.34	0.71	10.0	22,346
Basset 3	0.38	0.28	3.51	1.62	−9.58	6.94E-5	9.39	11,953
Cosby 1	0.33	0.28	2.88	0.66	2.21	9.2	5.40	221
Cosby 2	0.33	0.28	2.72	0.62	2.49	12	5.42	225
Vereecken 1	0.26	0.26	2.36	0.43	4.46	87	10.2	25,986
Vereecken 2	0.25	0.37	3.18	0.78	−3.25	0.049	7.29	1466
Wösten	0.31	0.28	10.5	3.53	−18.2	1.23E-8	6.30	546
Li	0.32	0.27	6.67	1.37	−3.26	0.038	18.1	699,357,420
Weynants	0.33	0.28	4.10	0.67	1.21	3.35	4.11	60.9
Wang	0.35	0.28	1.84	0.63	3.03	21	5.98	394
Observed data					**3.82**	**46**	**8.77**	**6406**

versa. The coefficients for bulk density in combination with silt in the Wang PTF or bulk density with clay (Wösten PTF) changed from negative to positive, while the coefficients for interaction terms for SOM and bulk density (Wösten PTF) as well as for SOC and elevation (Wang PTF) remained similar (Table S6b). The calibration of the principal components for prediction of *Ks* also resulted in different responses. The coefficients of PC1, which reflected coarse texture versus fine texture, and PC2, which reflected bimodality but not necessarily clay in the particle size distribution, were smaller after calibration compared to before calibration (Table 2, Table S5a). The regression coefficients of PC1, indicating coarse texture and PC5, an indication of clay content, were significant, those of PC1 and PC5, and PC6 changed from positive to negative, and those belonging to PC5 and PC6 (clay and slight bimodality in the particle size distribution) changed one order in magnitude (Table S5a).

The regression coefficients in the PTFs from Basset et al. (2023), which included soil structure, did not change direction, except for the intercept in Basset 1 and 2 that changed from negative to positive and changed one order in magnitude. The coefficients of the MWD term decreased one order in magnitude when calibrated to our data, and MWD had a significant effect on *Ks* in every calibrated Basset PTF ($p < 0.05$) tested. The same held true for the SOC term ($p < 0.01$). The coefficient for bulk density also decreased one order in magnitude, but was not significant after calibration of the regression coefficients (Table S6).

3.1.4. Performance of calibrated pedotransfer functions without soil structure

After calibration of the regression coefficients based to our measured data, the PTFs generally performed better with R^2 values ranging between 0.10 and 0.51 and RMSE values between 1.10 and 0.81 (ln(Ks)). Noteworthy, the improvement after calibration in the explained variation of the observed field measured *Ks* values was consistent throughout all existing PTFs (Fig. 4, Table 4).

The two Cosby PTFs, which used only textural information as inputs, performed the worst. The PTF of Li included SOM as well as soil texture and explained around twice as much of the variation in the data compared to the Cosby PTFs. The PTFs that included bulk density, next to SOM or SOC and texture, but did not consider interactions (i.e., the Vereecken 1 and Weynants PTF), showed similar performance to the PTF of Li, and explained around 30% of the variation in the data. The nonlinear PTF of Wang, which included interactions of bulk density and silt content as well as SOM and elevation, explained only 16% of the variation in the data, irrespective of the larger number of predictors. The nonlinear PTF of Wösten additionally included interactions of the bulk density and SOM, and used bulk density and clay as predictors. This PTF explained 48% of the variation in the data. The Vereecken 2 PTF had the highest performance among the existing PTFs, as it had the lowest RMSE and highest correlation based R^2. It included bulk density and SOM next to information on the variation in texture as well as the bimodality in soil texture due to the principal components describing soil texture as inputs. Nevertheless, best predictions were achieved when new regression equations (PTFs) were developed, with the PTFs A and C, which were also nonlinear and included interactions of the SOC, sand, and clay (Table S8), explaining more than half of the variation in the data.

The extent to which the individual PTFs were able to explain the variation in our data was also reflected in the range of predicted *Ks* values (Table 4). The two Cosby PTFs only predicted *Ks* in a range of 206–880 and 200–907 cm day^{-1} respectively, covering 51–53% of the measured data. In the slightly more complex PTFs, this range increased to around 63% for the Li and Vereecken 1 PTF, and to 67% for the Weynants PTF. The inclusion of interactions in the PTF of Wang and Wösten increased the maximum predicted *Ks* value to around 1588 and 1720 cm day^{-1}, respectively. The lowest *Ks* was predicted using the Wösten PTF with 60 cm day^{-1}, which was similar to the lowest value predicted by the Vereecken 2 PTF, and very similar to the PTFs of Li, Vereecken 1, and Weynants with 86, 91, and 63 cm day^{-1}, respectively, whereas the lowest predicted *Ks* value by the Wang PTF was 206 cm day^{-1}. Around 82% of the measured data fell into the prediction range of the Wösten PTF, and 63% fell into the prediction range of the Wang PTF. The range in prediction of the Vereecken 2 PTF (59–1620 cm day^{-1}) was slightly smaller than that of Wösten (60–1720 cm day^{-1}), but the range was very similar and around 80 and 82% of the measured data fell into this range, respectively. In contrast, PTF A and C had slightly higher predicted minimum *Ks* values (77 and 65 cm day^{-1}), but also higher predicted maximum *Ks* values (1901 and 3678 cm day^{-1}), covering 84 and 88% of the measured data (Table 4). Nevertheless, none of the PTFs covered the full range of observed *Ks* values.

After repeated 10-fold cross validation, most of the simple PTFs (Cosby, Vereecken 1 and Weynants) had higher R^2 values and slightly higher RMSE values (Table 4). The more complex PTFs, such as Vereecken 2 and Wösten had similar or slightly lower R^2 and higher RMSE values. The PTF of Li, Wang, PTF A, and PTF C had a higher R^2 and higher RMSE. Compared to the metrics of the PTFs that had seen all data, the three best performing PTFs were still PTF C, PTF A, and the Vereecken 2 PTF.

3.1.5. Calibrated pedotransfer functions that include soil structure

Among the five PTFs that include soil structural information as predictors, the PTFs Basset 1, 2, and 3 included the MWD, SOC, and bulk density only, while PTF B and D did not include bulk density but included clay content. PTF D also included the soil temperature and initial soil water content (Table S7). These different approaches resulted in different PTF performance (Fig. 4, Table 4). The Basset 1 PTF, which only included the MWD, performed the worst and only explained 10% of

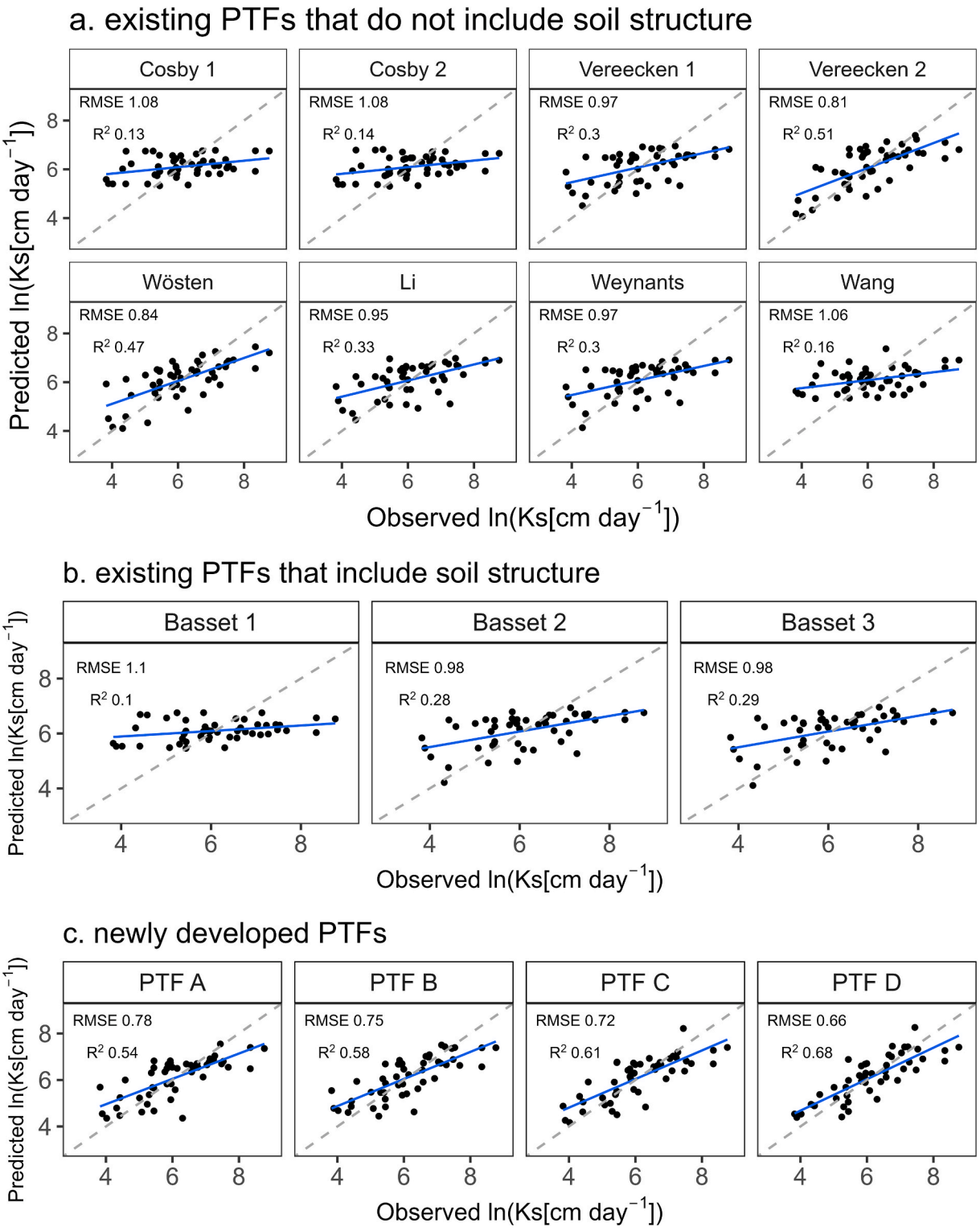

Fig. 4. Predictions of the measured saturated hydraulic conductivity (Ks) using existing, calibrated pedotransfer functions (PTFs) that do not include soil structural information (a), existing, calibrated PTFs that include soil structure (b), and the newly developed PTFs (c). RMSE = Root Mean Squared Error (ln(Ks) in cm day^{-1}), R^2 is the correlation based R^2 value. More information on the PTFs after 10-fold cross validation is given in Table 4. Blue lines display the regression line, whereas the grey dashed line displays the 1:1 line.

the variation in the data. When SOC, or SOC and bulk density were added as predictors such as in Basset 2 and Basset 3, the explained proportion of data variability increased to 28 and 29%, respectively. This PTF performance was similar to those of the calibrated Vereecken 1 and Weynants. The newly developed PTF B and D explained 58 and 68% of the variation and had the lowest RMSE among all PTFs that included soil structural information for *Ks* prediction. The better performance of PTF B compared to PTF A can be traced back to the inclusion of soil aggregation as predictor. Additionally, PTF B performed similarly well as PTF C, which did not include soil structural information but the initial

Table 4
Performance metrics for predicting Ks predictions using pedotransfer functions (PTFs), compared to the observed data, based on all data or using 10-fold cross validation (CV) with 100 repetitions as well as minimum and maximum of the saturated hydraulic conductivity (Ks) values with and without log (ln) transformation. R^2 = correlation based R^2, RMSE = Root Mean Squared Error (ln(Ks)), Ks = saturated hydraulic conductivity in cm day^{-1}, sd = standard deviation, AIC is the Akaike information criterion, BIC is the Bayesian information criterion. Results of PTFs in cursive are PTFs that include soil structure.

PTF	CV R^2		CV RMSE		AIC	BIC	Minimum		Maximum	
	Mean	sd	Mean	Sd			ln(*Ks*)	*Ks*	ln(*Ks*)	*Ks*
Existing PTFs that do not include soil structure										
Cosby 1	0.37	0.30	1.08	0.28	153	158	5.33	206	6.78	880
Cosby 2	0.35	0.30	1.11	0.30	154	162	5.30	200	6.81	907
Vereecken 1	0.38	0.29	1.04	0.30	148	159	4.51	91	6.95	1043
Vereecken 2	0.47	0.29	0.92	0.29	136	153	4.07	59	7.39	1620
Wösten	0.39	0.30	1.50	1.49	146	169	4.10	60	7.45	1720
Li	0.39	0.30	1.04	0.30	148	161	4.45	86	6.98	1075
Weynants	0.42	0.29	1.00	0.29	146	155	4.14	63	6.92	1012
Wang	0.31	0.29	1.20	0.29	159	172	5.33	206	7.37	1588
Existing PTFs that do include soil structure										
Basset 1	*0.39*	*0.31*	*1.10*	*0.30*	*154*	*160*	*5.46*	*235*	*6.76*	*863*
Basset 2	*0.43*	*0.29*	*1.00*	*0.29*	*145*	*153*	*4.21*	*67*	*6.94*	*1033*
Basset 3	*0.41*	*0.30*	*1.01*	*0.29*	*147*	*157*	*4.11*	*61*	*6.96*	*1054*
PTFs developed in this study										
PTF A	0.59	0.27	0.83	0.29	129	142	4.35	77	7.55	1901
PTF B	*0.62*	*0.25*	*0.83*	*0.25*	*127*	*142*	*4.44*	*85*	*7.50*	*1808*
PTF C	0.60	0.26	0.83	0.25	125	142	4.17	65	8.21	3678
PTF D	*0.68*	*0.22*	*0.79*	*0.19*	*118*	*137*	*4.39*	*81*	*8.26*	*3866*
Observed data							**3.82**	**46**	**8.77**	**6406**

soil water content and temperature. Overall, PTF D, which included soil structure, SOC content, clay content, initial soil water content, and soil temperature as predictors, performed best amongst all PTFs.

In line with the results for the coefficient of determination, also the range of predicted *Ks* was lowest for the Basset 1 PTF amongst all PTFs tested, and only 37% of the measured data fell within the predicted *Ks* range. After including SOC, or SOC and bulk density as predictors, the predicting range improved to 69%, similar to the Weynants PTF. PTF B and D predicted *Ks* values in a range of 78% and 86% of the measured data, respectively.

After repeated cross validation, the R^2 values of the Basset PTFs increased and the RMSE only changed slightly (Table 4). PTF B and D had slightly lower R^2 values and higher RMSE values after repeated cross validation. Out of all PTFs tested, PTF C and D performed best and provided largest prediction accuracy and data coverage. They also seemed most stable, as their cross validated RMSE was the lowest compared to the other PTFs.

3.2. Soil aggregates

To overcome a lack of MWD data in field studies that could be used as predictor for *Ks* estimation, additional PTFs were developed to predict the MWD from easily to obtain soil properties. In total four different regression based PTFs were developed to predict the MWD (Tables S4 and S8). All four PTFs showed a decreasing MWD with increasing sand content. When the PTFs included clay content in combination with bulk density, a positive interaction was found, and we observed a positive interaction of SOC and clay as well. The effect of soil initial water content measured in the field also had a positive effect on MWD. There were no significant effects of WRB soil group (Table S8).

All four PTFs tested to predict the MWD explained 87–92% of the variation in the MWD data and had an RMSE of 374–289 μm in MWD (Fig. 5). MWD_PTF 1 predicted MWD values within the range of measured MWD ones, MWD_PTF 2 predicted slightly larger MWD values than observed, whereas MWD_PTF 3 and 4 predicted physically illogical

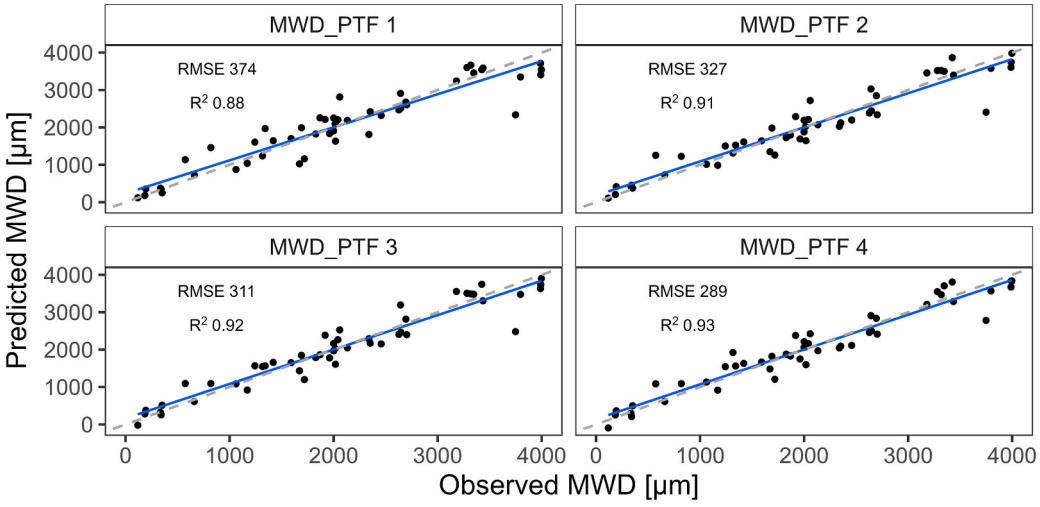

Fig. 5. Observed mean weight diameter (MWD) of the aggregates and performance of the pedotransfer functions (PTFs) for predicting MWD, based on the training on the whole dataset. RMSE = Root Mean Squared Error, R^2 is the correlation based R^2 value. More information on the PTFs after 10-fold cross validation is given in Table 5. Blue lines display the regression line, whereas the grey dashed line displays the 1:1 line. MWD_PTF 3 and MWD_PTF 4 are predicting negative MWD values and are thus not recommended for use.

negative MWD values (−22 and −95, Table 5), and are thus not recommended for use.

The repeated *k*-fold cross validation ($k = 10$) showed that the RMSE of MWD_PTF 2 and 3 was lowest and their R^2 was the highest among the four PTFs (Table 5). When the RMSE of the cross validation was compared with the RMSE of PTFs trained on the whole data set, MWD_PTF 3 and 4 had higher RMSE (3.2 and 36.3% respectively) after cross-validation, which indicated over-fitting for MWD_PTF 4 and slight overfitting for MWD_PTF 3, whereas MWD_PTF 1 and 2 had a slightly lower RMSE after cross validation, of −1.1 and −0.1%. Also, the R^2 value of MWD_PTF 1, 2, and 3 was slightly higher after cross validation, except for MWD_PTF4, where the R^2 was lower. Based on the performance statistics discussed, MWD_PTF 2 was used to further optimize the *Ks* prediction.

3.3. Predictions of the saturated hydraulic conductivity using estimated aggregate MWD values

In a next step, we evaluated the performance of the PTFs that predicted *Ks* and included the MWD as a predictor in the regression, with either measured MWD values or estimated MWD values predicted using the best performing MWD_PTF (MWD_PTF 2 (Fig. 5)). The regression coefficients of the Basset 1–3 PTFs, and PTF B and D were not recalibrated to the newly predicted MWD values. As can be seen in Fig. 6, using predicted MWD in *Ks* predictions yielded comparable results to using measured MWD for the *Ks* prediction for the PTFs tested. In all cases, the correlation based R^2 exceeded 0.91 and the RMSE ranged between 0.11 and 0.23 ln*Ks* (cm day^{-1}).

After 10-fold cross validation, PTF B and D were performing better than the Basset PTFs (Fig. S2, Table S9). Compared to PTFs that used measured MWD values, the RSME was lower for the calibrated Basset PTFs and the newly developed PTFs B and D. The three Basset PTFs predicted 37, 67, or 69% of the *Ks* values measured for Basset 1, 2, and 3 respectively. For Basset 1 and Basset 3, the range stayed the same when using the estimated MWD values compared to using the measured MWD values, but this was 2% lower for Basset 2. PTF B and D predicted 76 and 84% of the range of observed *Ks* values, respectively, which was 2% lower compared to the range of predicted Ks values of PTF B and D that used measured MWD values.

4. Discussion

4.1. Estimating saturated hydraulic conductivity Ks

Pedotransfer functions are empirical models whose ability to accurately predict *Ks* depends on the data they have been trained on and the data they will be applied to (Fuentes-Guevara et al., 2022; Nemes et al., 2003; Schaap and Leij, 1998). Fuentes-Guevara et al. (2022) pointed out that not necessarily the pedoclimatic conditions, but rather the data similarity between data used to build the PTFs and those that the PTFs will be applied to plays a crucial role in how the PTFs perform. Similarity can be described by the correlations, but also the spread, variance, and extremes within the datasets. Since the original training data of the existing PTFs can be unavailable or unknown, the existing PTFs sometimes fail to predict the hydraulic characteristics or other soil properties accurately when they are applied to new data; therefore, calibration of PTFs has been suggested (Khodaverdiloo et al., 2022; Szabó et al., 2021). After calibration, the regression coefficients can turn from positive to negative or even change by several orders of magnitude after calibration as reported by Báťková et al. (2023), which was also found in our study. Pedoclimatic conditions and similarity between the dataset used in this study and those of the existing PTFs tested in this study varied. The US database of Cosby et al. (1984), the European HYPRES database (Wösten et al., 1999), and the database from Wang et al. (2012) from the Loess plateau in China, generally contain datapoints with finer soil texture than our samples. Our dataset also shows on average higher SOC content than those reported in HYPRES, as well as those used by Li et al. (2007) and Wang et al. (2012). In contrast, the Belgian dataset used by Vereecken and Weynants was fairly similar to ours. The Weynants PTF is known to underestimate *Ks* as it has been built to predict near saturated hydraulic conductivity K^*, which can be observed in the small range in predicted *Ks* values before calibration to our data. On the other hand, the Vereecken 2 PTF performed best of all existing PTFs before calibration, which could be due to similarity of the datasets. Another reason could be that the Vereecken 2 PTF includes information from principal components derived from soil texture information of our dataset, and therefore, is already to some extent adjusted to our dataset, compared to the other PTFs taken from literature. Therefore, the poor performance of the uncalibrated PTFs could be due to the lack of similarity between datasets, e.g., that the datasets for development for the existing PTFs vary in soil texture or SOC contents. Furthermore, some variables, such as SOC content, might be distributed normally that were not normally distributed in our data or vice versa, which then leads to differences in correlations in the dataset used for development compared to our data and results in poor PTF performance, especially without calibration (Arbor et al., 2023; Fuentes-Guevara et al., 2022; Shi et al., 2026). In general, it is known that calibrating the regression coefficients of the PTFs results in a better fit, as differences in datasets might cause biases in the predictions (Báťková et al., 2023; Nemes et al., 2003; Schaap and Leij, 1998), therefore, it is not surprising that the calibration of the PTFs used in this study yielded better results compared to the original formulation.

Furthermore, all PTFs tested have been developed using the US soil texture classification, which defines the grain size of sand between 2000 and 50 μm. In some (European) countries, for example Germany, but also in the IUSS system, the lower threshold for sand is set to 63 μm (Nemes et al., 1999). Therefore, changing from 50 μm to 63 μm sand particle size might introduce some error in the PTF predictions, as the silt fraction will become larger while the sand fraction will become smaller. One alternative to deal with those different thresholds is the use of interpolation procedures to convert one threshold to another, although this procedure is prone to errors (Nemes et al., 1999; Wösten et al., 1999). A second alternative is to calibrate the regression coefficients of the existing PTFs and make them suitable to be used for the textural inputs available. We decided to take the latter approach to be able to compare existing PTFs with newly developed ones (PTF A-B); which has also been done by Schoch et al. (2025) and Khodaverdiloo

Table 5
Mean weight diameter (MWD) pedotransfer function (PTF) performance metrics, compared to the observed data, after k-fold cross validation with k = 10 and n = 100. RMSE = Root Mean Squared Error in μm mean weight diameter (MWD), sd = standard deviation, R^2 = correlation based R^2, AIC is the Akaike information criterion, BIC is the Bayesian information criterion. MWD_PTF 3 and MWD_PTF 4 are predicting negative MWD values and are thus not recommended for use.

PTF	CV RMSE		CV R^2		AIC	BIC	Minimum	Maximum
	Mean	sd	Mean	sd			MWD (μm)	MWD (μm)
MWD_PTF 1	370	165	0.90	0.12	730	739	118	3712
MWD_PTF 2	324	144	0.92	0.09	718	730	110	3981
MWD_PTF 3	321	136	0.93	0.09	716	729	−22	3903
MWD_PTF 4	394	162	0.88	0.14	722	749	−95	3835
Observed data							**118**	**3997**

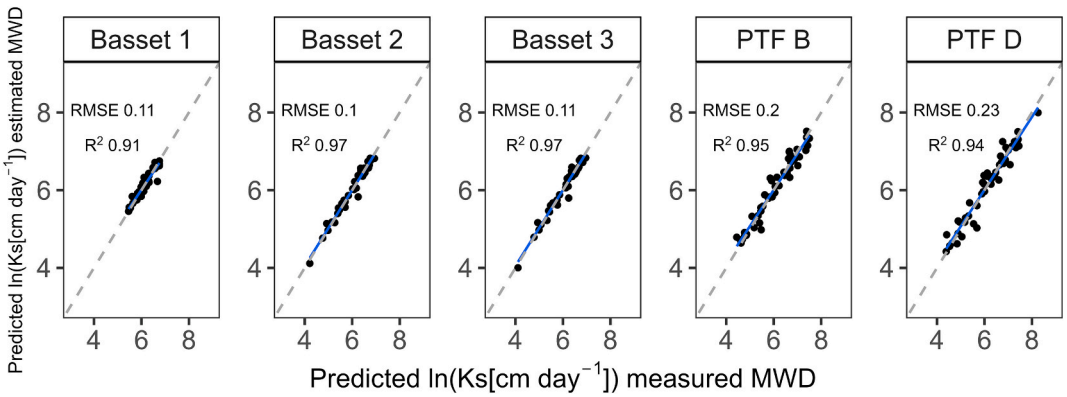

Fig. 6. Predictions of the saturated hydraulic conductivity (Ks) using pedotransfer functions (PTFs) that include soil structure, with measured aggregate mean weighted diameter(MWD) values and estimated MWD values. RMSE = Root Mean Squared Error. Blue lines display the regression line, whereas the grey dashed line displays the 1:1 line.

et al. (2022), and is advised for the work with smaller datasets.

The most notable difference after calibration was observed for the sand content coefficients, which were often initially positive (e.g., in Cosby, Wösten, Weynants, and Wang PTFs), but turned negative when calibrated to our data. Aside from the definition of the grain size of sand, this can also be explained by the different measurement methods for *Ks*. Most of the existing PTFs that were tested in this study were based on laboratory *Ks* measurements. It is known that the method used to measure *Ks* can lead to different *Ks* results on the same soil, since laboratory measurements are based on smaller soil volumes compared to most infiltrometer field measurements (Rahmati et al., 2018). Therefore, it is likely that individual macropores are underrepresented in laboratory measurements (Fodor et al., 2011). It has been also shown, that samples with greater length and diameter, thus larger volume, exhibit higher *Ks* values (Ghanbarian et al., 2015). This can then in turn lead to inaccurate estimations of field measured *Ks* as the effect of soil structure might be underestimated when using PTFs that only use basic soil properties such as texture and are developed based on laboratory *Ks* measurements (Rahmati et al., 2018). PTFs that were developed to predict the lower, laboratory measured *Ks* values, might thus also predict lower field measured *Ks* values before calibration due to this underestimation of soil structure that might be less common in field measured *Ks*. PTFs that were developed on laboratory *Ks* measurements, might in turn predict higher *Ks* with higher sand content, which this was be the opposite in field measured *Ks* where generally lower *Ks* values were measured in sandy soils. This might have been caused by ineffective saturation due to hydrophobicity, which can be managed in the laboratory *Ks* measurements. Both the higher than expected *Ks* on fine textured soils due to the underestimation of soil structure in laboratory measurements and lower than expected *Ks* due the effect of hydrophobicity can cause the uncalibrated PTF developed on laboratory *Ks* to predict "the opposite" of what was measured in the field and thus result in negative correlations between observed and predicted *Ks*.

When soil structure, but not soil texture is included as inputs in PTFs, like those developed by Basset et al. (2023), this effect between laboratory measured and field measured *Ks* was smaller and they correlated positively, because the soil structure effect was included and effect of texture on the laboratory measured *Ks* was excluded. The three Basset PTFs generally predicted higher *Ks* with higher MWD rather than high *Ks* for coarse textured soil or low *Ks* for fine textured ones. Even though the slope was positive in the original Basset PTFs, they were still not able to estimate *Ks* precisely before calibration. Since all existing PTFs improved after calibration of the regression coefficients on own data, the first hypothesis that calibration of the regression coefficients is necessary in order to have more accurate predictions of field measured *Ks* can be accepted.

Even after calibration of the regression coefficients to our own data, the newly developed PTFs (PTF A, B, C, and D) outperformed the reported PTFs. The best performing reported PTF after calibration was the Vereecken 2 PTF, which had *Ks* predictions and RMSE and R^2 values very similar to those of the newly developed PTF A (Fig. 4, Table S2), which was the simplest PTF developed. The Vereecken 2 PTF and PTF A both include interaction of different textural fractions. PTF A represents the interaction of sand and clay, while the Vereecken 2 PTF used principal components (Vereecken et al., 1990). In general, the interaction terms represent bimodality in the particle-size distribution, and thus, mimic the effect of a soil structure predictor. Both PTFs, however, do not include direct indicators of soil aggregation, which likely lead to limited accuracy in predicting high *Ks* values (Fig. 4), as those high *Ks* values are commonly associated with water flow in macropores or larger pores between macroaggregate units.

PTF B and D performed better than PTF A, which is due to the combination of soil structure and soil texture information as inputs, thus reflecting the contribution of both texture- and structure-derived pore spaces to *Ks*. This has also been reported in other studies. For example, Basset et al. (2023) compared different PTFs predicting steady state infiltration rates (which we did not include in this study) and observed, that those PTFs performed best that included soil texture but also additionally the aggregate MWD and SOC content.

We thus conclude, that a combination of soil structure and soil textural information, as well as SOM or SOC is necessary to obtain best *Ks* predictions. The improvement of the PTF performance after including soil aggregation can be attributed to the fact that aggregate size can be a specific indicator for structural pores formed in-between the aggregates (Arrington et al., 2013; Bonilla et al., 2008), which are especially relevant for water flow in (near) saturated conditions (Vereecken et al., 2022). The finding supports our second hypothesis, as including information on soil structure, here MWD, in the PTFs besides texture and SOC will help to better predict *Ks*.

In this study, we used the aggregate size (MWD) as a surrogate for soil structure, that can both be estimated and measured relatively easily compared to other surrogates for soil structure such as porosity. Soil structure, however, is more complex than the size of the aggregates, and it should be kept in mind that destructive analyses of soil structure such as wet sieving also have drawbacks (Rabot et al., 2018). Soil aggregate size (MWD) by itself could only explain a small part of the variability in *Ks*, and does not directly reflect the type of aggregate distribution, the porosity, pore connectivity, or flow tortuosity. Further research could focus on how these aspects of soil structure are connected and how they relate to *Ks* predictions.

4.2. *Including predictions of soil aggregation into PTFs*

Measuring soil aggregation or other soil structure parameters is time-

consuming, labour-intensive, and costly. PTFs for aggregation could be developed using existing aggregate databases (Sarkar et al., 2023), and these PTFs could then be included in *Ks* predictions. However, there are currently not many continental or global databases on soil aggregation available and even less PTFs that allow estimation of structural information like MWD on a large scale (Purushothaman et al., 2022). For example, Araya and Ghezzehei (2019) tested several PTFs and machine learning algorithms on the USKSAT database (Pachepsky and Park, 2015) and included bulk density and SOC content as proxies for soil structure. The best approach for predicting soil hydraulic parameters using a European database (EU-HYDI) (Weynants et al., 2013) was to include pH and cation exchange capacity as surrogates of soil structure (Tóth et al., 2015), as they carry information on clay minerals and SOM content (Totsche et al., 2018).

In our study, we built four PTFs to predict the MWD of the soil aggregates by soil texture, bulk density, and SOC content information. In those four PTFs, the largest improvement in prediction accuracy occurred after including the interaction of clay and SOC. After cross validation, the RMSE decreased, R^2 increased, and standard deviation of these metrics decreased, indicating stability. Additionally, the range of prediction was most similar to the range of MWD values observed.

The interaction of SOC and clay contents allowed for prediction of greater MWD, as fine textured soil, especially clayey soils, are often associated to higher SOC content and higher MWD (Blanco-Canqui and Lal, 2004). Both are seen as major drivers of soil aggregation, which is attributed to the fact, that soil aggregates are built up of organic matter that is “glued” to mineral particles (Kaiser and Guggenberger, 2003).

In general, the range of prediction of the MWD was large and accurate. However, both MWD_PTF 3, which included the initial soil water content, as well as MWD_PTF 4, which included the initial soil water content and the WRB soil group, predicted physically illogical negative MWD values. Additionally, cross validation showed, that after adding the initial soil water content and/or the WRB soil group, both MWD_PTF 3 and MWD_PTF 4 were prone to overfitting. For our current study, which is based on a relatively small data set, we therefore rather rely on a simpler PTF (i.e., MWD_PTF 2) to estimate soil aggregate MWD and do not recommend MWD_PTF 3 and 4 for use.

Noteworthy, the PTFs for the prediction of *Ks* that used estimated MWD values performed slightly better or similar than those that used measured MWD values, as they had a lower RSME, higher R^2 and improved PTF fit after cross validation. The effect of including estimated MWD values into the *Ks* PTF was the same as for the PTFs derived by Basset et al. (2023) and the newly developed PTFs B and D. Nevertheless, it needs to be considered that despite an R^2 of 0.9 of the PTFs for the estimation of the MWD, some MWD values were not predicted accurately, which might lead to less heterogeneity in the predicted soil structure variables (MWD) compared to the measured ones. Therefore, the PTFs that predicted *Ks* based on estimated rather than measured MWD may have performed better due to a certain level of noise reduction in the soil structure data input (MWDs). Since soil structure is a spatially and temporally varying soil property, lower heterogeneity might omit important information (Jirků et al., 2013; Ye et al., 2018). Hence, a trade-off between information gain and noise reduction has to be made. In our current study, we thus have to reject our third hypothesis that including estimated aggregate MWD leads to lower PTF performance for *Ks* prediction compared to PTFs where measured soil structure inputs will be used. Further research could therefore focus on how well the newly developed MWD PTFs perform on independent datasets, and how these results vary with respect to soil texture, the type of sand correction used in the MWD measurements, or after conducting different lab methods for the MWD such as comparing wet sieving and density fractionation. It has to be noted that these PTFs were developed on a dataset with a maximum clay content of 32%, since clay content is included on its own and as interactions in both MWD_PTF 1 and 2, predictive power might decrease in soils with high clay content. Aside from the error from of the MWD term and interaction terms that include the aggregate MWD, the error for *Ks* predictions can also be caused by the clay term and interactions with clay, since the *Ks* PTFs were not trained on soils with high clay content either. These might strongly increase the RMSE. We therefore do not recommend using these PTFs on soils with high clay content and highlight the need for extended data bases for validation of the MWD PTFs.

The error from the MWD PTF predictions could further be propagated to the *Ks* PTFs that included the aggregate MWD as a predictor (Basset PTFs, PTF B, and PTF D). Based on the current dataset, MWD_PTF 1 and 2 had an RMSE of 366 and 326 cm day^{-1} respectively. The risk of error propagation would thus increase with increasing RMSE of the MWD PTFs, but additionally depends on the *Ks* PTF that they are included in. The effect of false aggregate MWD estimations would be larger in PTF B and PTF D than the Basset PTFs, as PTF B and D include more aggregate MWD-terms, of which some interact with other predictors. We therefore advise to use measured aggregate MWD values if they are available and again emphasize validation of the MWD PTFs using larger databases.

4.3. Influence of soil water content and temperature

This study includes field measured *Ks* on a European temperature and SOC gradient with varying soil water contents during infiltration measurement. Tension infiltrometer measurements, such as those performed by the mini disk infiltrometer, can be affected by the initial soil water content (Matula et al., 2015). Hood infiltrometers such as those used in our study seemed to be less affected by the initial soil water content compared to mini disk infiltrometers, which is likely due to difference in the order of the tension sequence used during measurements (Matula et al., 2015; Schwärzel and Punzel, 2007). In our dataset, three quarters of our measured initial soil water contents were below 20% volumetric water content, which is lower than the range (24–38%) measured by Matula et al. (2015). Additionally, some of the soils in our study showed high degrees of hydrophobicity, and therefore, lower hydraulic conductivities. This explains the positive regression coefficient of the soil water content in the newly developed PTF C and D, as well as the higher R^2 and lower RMSE compared to PTF A and B, which are based on the same inputs but exclude the measured soil water content and soil temperature. At lower soil water contents, hydrophobicity in soils can occur, especially in sandy or organic rich soil or at specific pH (Dekker et al., 2001; Popović and Cerdà, 2023). In case of low soil water contents and high hydrophobicity, only part of the entire flow paths can contribute to the overall water flow (e.g. when fingering occurs), and therefore, even at steady-state-infiltration the hood infiltrometer data might be biased. This problem has been observed by Buczko et al. (2006), where hood infiltrometers measured *Ks* were one magnitude lower than those performed by a ring infiltrometer. They also pointed out, that this is especially true for measurements taken in summer, as drought periods can enhance soil hydrophobicity. Other effects of soil water content differences can be attributed to shrinking and swelling of clay minerals, which might lead to changes in soil porosity during the measurements, and thus, lower than expected *Ks* on fine textured soils, as reported by Hardie et al. (2012). Therefore, including soil water content as a predictor in PTFs seems logical in order to capture the seasonal variations of *Ks* and soil structure (Hardie et al., 2012; Schoener and Stone, 2019).

Climatic variables often influence the hydraulic conductivity, and therefore, weather variations at the time of the infiltration measurements can explain a part of the large variance observed in field measured *Ks* (Jorda et al., 2015). Additionally, laboratory *Ks* measurements are mostly performed on fully saturated soils, where hydrophobicity especially in sandy or organic rich soils does not play a role as the matrix will be already fully wetted. This is not the case during field measurements, where the soil can be more or less dry, and therefore, also partly hydrophobic. Even if for the calculation of *Ks* by the infiltrometer data only the steady-state infiltration will be used, hydrophobicity effects cannot

be excluded as mentioned already, leading to lower *Ks* values compared to those measured under full saturation in the laboratory.

Soil water content also played a role in the MWD based PTFs, as they yielded a better fit when actual soil water content was included as an additional input variable (MWD_PTF 3 and MWD_PTF4), whereby higher soil water content is associated with larger MWD. Similar results were found on another European climate transect by Edlinger et al. (2023), who found that after accounting for the effect of land use, the aridity index and clay content were key factors for soil aggregation. They also stated that at arid sites soil aggregates had a smaller MWD than those from less arid ones, which was associated with lower SOC contents at arid sites. This is also reflected by a positive regression coefficient of the soil water content term in MWD_PTF 3 and 4, which indicates that dry soils are associated with lower MWD. However, as noted in chapter 4.2, these PTFs estimated negative MWD values and were prone to overfitting and are not recommended for use. The overfitting, might be due to the large variation of the data and the fact that this variable reflects the conditions during sampling. During aggregate fractionation in the laboratory, the samples were rewetted with water, and with ethanol in hydrophobic samples, therefore the initial soil water content during sampling might not affect the laboratory analysis in the same way as it might have affected the infiltration measurement in the field. In this case the initial soil water content might help to explain the observed differences in aggregation among our sites, but might not be as useful for MWD prediction purposes.

Soil temperature is also known to affect the hydraulic conductivity, as higher temperatures make water less viscous and can lead to higher hydraulic conductivities. Usually lab hydraulic conductivities are therefore normalized to soil temperatures at 20 °C (Holthusen et al., 2012), but in the field the hydraulic conductivity can be around three times higher at 25 °C compared to those measured at 10 °C (Ren et al., 2014). This large difference is not only caused by viscosity changes but also by the thermal dependence of swelling of soil particles and changes of the surface tension of the water and the interaction between water and matrix (Gao and Shao, 2015; Levy et al., 1989). Another effect of soil temperature is rather indirect as with increasing temperatures macropores might dry out and become air filled. This air can be entrapped during fast infiltration, and therefore, lower measured infiltration rates (Gao and Shao, 2015). In our measurements, soil temperature ranged from 8 to 37 °C (mean 23 ± 8 °C), which could have partly affected the variability in *Ks* measurements.

A key challenge in predicting field measured *Ks* by PTFs relies in its dynamic nature (Alletto et al., 2015; Kreiselmeier et al., 2020). Using only static soil properties such as texture in a PTF excludes the temporal variation of field measured *Ks* due to seasonal variation in soil structure (Kreiselmeier et al., 2020). SOC and aggregate MWD are at least in part dynamic and are, thus, likely more suited to predict dynamic *Ks* when they are included in PTFs. SOC only varies slightly on seasonal time scale and is mainly associated to land-cover, management history and is often correlated to soil texture (Schillaci et al., 2017). The aggregate MWD in turn is a parameter connected to soil porosity, and thus, directly linked to soil structure. In how far the temporal variations of soil aggregation and MWD match those of *Ks*, however, still warrants investigation. In this study, the aggregate MWD and SOC were not measured as dynamic soil properties, like we did with the soil water content and soil temperature.

To be able to compare field measured *Ks* across the climate gradient and incorporate local anomalies during the time of measurement, soil water content and soil temperature were included in PTF development. By including the soil water content and soil temperature at the time of the measurement, this might not reflect the general climate of our sampling sites, but rather the state of the weather during the measurement. Soil water content and soil temperature are both highly dynamic in space and time and fluctuate seasonally, as well as diurnally, since they are affected by soil management, vegetation, topography and atmospheric states such as by precipitation, atmospheric temperature, solar radiation (Mohanty, 1998; Santanello et al., 2007). Field measured *Ks* can be impacted by variations in soil water content (Zhou et al., 2008) and associated potential hydrophobicity and matric potential driving the infiltration front, but also by swelling of clay particles (Hardie et al., 2012). As the impact of swelling of clays on *Ks* remains largely unknown (Ugarte Nano et al., 2015), including this process seems problematic. Changes in matric potential due to changes in initial water contents is on the other hand negligible as *Ks* was calculated from steady-state infiltration rates measured by a hood infiltrometer. Still, some uncertainties will be introduced by neglecting the above-mentioned effects.

Nevertheless, as already discussed for the MWD PTFs, potentially high spatiotemporal variation in soil water content and the lack of a larger data base to verify the influence of soil water content and temperature during field measurements, hinders detailed analysis of these confounding factors. Further research and more data are likely needed to quantify the risk of overfitting of PTF C and PTF D, as they use third order interactions and have a relatively large number of predictors compared to the size of the dataset that we used in this study. In addition, we highlight the need for systematic data collection of the antecedent soil water content and soil temperature in combination with field measured *Ks*, which is already recognised but rarely done (Jorda et al., 2015; Rahmati et al., 2018), to validate these dynamic PTFs. Therefore, we currently recommend to use PTFs that are independent of soil water content and soil temperature when including soil structure information in PTFs.

5. Conclusion

This study showed that the best PTF-based estimates of field measured *Ks* were obtained when using a combination of information on soil texture, SOC content, and aggregate MWD. We chose the MWD of the soil aggregates as a surrogate for soil structure, since this is one of the more cost effective and least labour intensive methods compared to other methods for measuring soil structure. The PTF prediction further improved when input data reflecting field conditions at the time of *Ks* measurement were included, such as initial soil water content and soil temperature. Nevertheless, the measurements of MWD remain time consuming and tedious, and as MWD are classically not reported in available soil hydraulic databases, we also developed a PTF to estimate MWD from easily available input data such as SOC, bulk density, sand and clay content. This PTF was able to predict the measured MWD with high accuracy ($R^2 > 0.9$). When the PTF-predicted MWD was fed into the existing or developed PTFs to predict field measured *Ks,* the prediction performance even increased compared to the direct use of measured MWD, likely due to the reduction of outliers and noise. We therefore suggest to include soil aggregate size (MWD) information into PTFs along with information on soil texture and SOC as MWD can substantially improve the estimations of *Ks*, whereby the direct measurements of MWD can be circumvented by using the developed PTFs. Field measured Ks is a highly dynamic soil property and its prediction can benefit from including antecedent soil water content and soil temperature as well, although this has to be validated first and we therefore suggest to only include soil aggregate size for now.

CRediT authorship contribution statement

D.J. Burger: Writing – original draft, Visualization, Validation, Software, Methodology, Investigation, Formal analysis, Data curation, Conceptualization. **W. Amelung:** Writing – review & editing, Supervision, Resources, Project administration, Methodology, Funding acquisition, Conceptualization. **A.P. Heidtmann:** Writing – review & editing, Investigation, Formal analysis. **M.S. Geske:** Writing – review & editing, Investigation, Formal analysis. **H. Schimmel:** Writing – review & editing, Resources, Investigation, Formal analysis, Data curation. **M. Andersson:** Writing – review & editing, Resources. **J. Cobos Sabate:** Writing – review & editing, Resources. **R. Díaz Delgado:** Writing –

review & editing, Resources. **P. Gundersen:** Writing – review & editing, Resources. **M. Ibañez:** Writing – review & editing, Resources. **K.H. Jensen:** Writing – review & editing, Resources. **M.C. Looms:** Writing – review & editing, Resources. **P.E. Redondo-Hasselerharm:** Writing – review & editing, Resources. **A. Rico:** Writing – review & editing, Resources. **M.T. Sebastià:** Writing – review & editing, Resources. **S. Spielvogel:** Writing – review & editing, Resources. **L. Vesterdal:** Writing – review & editing, Resources. **J. Wallsten:** Writing – review & editing, Resources. **J. Westin:** Writing – review & editing, Resources. **S. Zacharias:** Writing – review & editing, Resources. **I. Zimmerman:** Writing – review & editing, Resources. **L. Weihermüller:** Writing – review & editing, Supervision, Resources, Methodology, Conceptualization. **H. Vereecken:** Writing – review & editing, Supervision, Resources, Project administration, Methodology, Funding acquisition, Conceptualization. **S.L. Bauke:** Writing – review & editing, Supervision, Resources, Project administration, Methodology, Investigation, Funding acquisition, Conceptualization.

Declaration of competing interest

The authors declare that they have no known competing financial interests or personal relationships that could have appeared to influence the work reported in this paper.

Acknowledgements

We would like thank all collaborators and farmers who granted access to their field sites. We thank S. Thienhaus and Dr. A. Wolf from RheinEnergie AG for providing us with information and access to the field sites in Cologne-north. We would further like to acknowledge K. Unger, F.S. Böttcher, M. Pieters, S. Turtle, J. Küls, T. Kaiyrbekov, K. Hövelmann, L. Kübler, and S. Pätzold for their assistance during field work, as well as M. Pieters, N.C. Przibille, A. Lindecke, and A. Langen for their assistance in the laboratory. This study was funded by the German Research Foundation (DFG), SFB 1502/1-2022, project number 450058266. This study has been made possible by data provided by Röbäcksdalen Field Research Station within the Swedish Infrastructure for Ecosystem Science (SITES).

Appendix A. Supplementary data

Supplementary data to this article can be found online at https://doi.org/10.1016/j.geoderma.2026.117911.

Data availability

Data is available as Supplementary material.

References

Ahuja, L.R., Cassel, D.K., Bruce, R.R., Barnes, B.B., 1989. Evaluation of spatial distribution of hydraulic conductivity using effective porosity data. Soil Sci. 148 (6), 404–411.
Alletto, L., Pot, V., Giuliano, S., Costes, M., Perdrieux, F., Justes, E., 2015. Temporal variation in soil physical properties improves the water dynamics modeling in a conventionally-tilled soil. Geoderma 243–244, 18–28.
Araya, S.N., Ghezzehei, T.A., 2019. Using Machine Learning for Prediction of Saturated Hydraulic Conductivity and its Sensitivity to Soil Structural Perturbations. Water Resour. Res. 55 (7), 5715–5737.
Arbor, A., Schmidt, M., Saurette, D., Zhang, J., Bulmer, C., Filatow, D., Kasraei, B., Smukler, S., Heung, B., 2023. A framework for recalibrating pedotransfer functions using nonlinear least squares and estimating uncertainty using quantile regression. Geoderma 439, 116674.
Arrington, K.E., Ventura, S.J., Norman, J.M., 2013. Predicting Saturated Hydraulic Conductivity for estimating Maximum Soil Infiltration rates. Soil Science Soc of Amer J 77 (3), 748–758.
Basset, C., Abou Najm, M., Ghezzehei, T., Hao, X., Daccache, A., 2023. How does soil structure affect water infiltration? a meta-data systematic review. Soil Tillage Res. 226, 105577.
Báťková, K., Matula, S., Miháliková, M., Hrúzová, E., Abebrese, D.K., Serdar Kara, R., Almaz, C., 2023. Prediction of saturated hydraulic conductivity Ks of agricultural soil using pedotransfer functions. Soil Water Res. 18 (1), 25–32.
Blanco-Canqui, H., Lal, R., 2004. Mechanisms of Carbon Sequestration in Soil Aggregates. Crit. Rev. Plant Sci. 23 (6), 481–504.
Bonilla, C.A., Norman, J.M., Molling, C.C., Karthikeyan, K.G., Miller, P.S., 2008. Testing a Grid-Based Soil erosion Model across Topographically complex Landscapes. Soil Science Soc of Amer J 72 (6), 1745–1755.
Buczko, U., Bens, O., Hüttl, R.F., 2006. Water infiltration and hydrophobicity in forest soils of a pine–beech transformation chronosequence. J. Hydrol. 331 (3–4), 383–395.
Caplan, J.S., Giménez, D., Hirmas, D.R., Brunsell, N.A., Blair, J.M., Knapp, A.K., 2019. Decadal-scale shifts in soil hydraulic properties as induced by altered precipitation. Sci. Adv. 5 (9), eaau6635.
Cosby, B.J., Hornberger, G.M., Clapp, R.B., Ginn, T.R., 1984. A Statistical Exploration of the Relationships of Soil Moisture Characteristics to the Physical Properties of Soils. Water Resour. Res. 20 (6), 682–690.
Dekker, L.W., Doerr, S.H., Oostindie, K., Ziogas, A.K., Ritsema, C.J., 2001. Water Repellency and critical Soil Water Content in a Dune Sand. Soil Science Soc of Amer J 65 (6), 1667–1674.
Diaz-Zorita, M., Perfect, E., Grove, J.H., 2002. Disruptive methods for assessing soil structure. Soil Tillage Res. 64 (1–2), 3–22.
Doerr, S.H., 1998. On standardizing the 'Water Drop Penetration Time' and the 'Molarity of an Ethanol Droplet' techniques to classify soil hydrophobicity: a case study using medium textured soils. Earth Surf. Process. Landforms 23 (7), 663–668.
Edlinger, A., Garland, G., Banerjee, S., Degrune, F., García-Palacios, P., Herzog, C., Pescador, D.S., Romdhane, S., Ryo, M., Saghaï, A., Hallin, S., Maestre, F.T., Philippot, L., Rillig, M.C., van der Heijden, M.G.A., 2023. The impact of agricultural management on soil aggregation and carbon storage is regulated by climatic thresholds across a 3000 km European gradient. Glob. Chang. Biol. 29 (11), 3177–3192.
Fatichi, S., Or, D., Walko, R., Vereecken, H., Young, M.H., Ghezzehei, T.A., Hengl, T., Kollet, S., Agam, N., Avissar, R., 2020. Soil structure is an important omission in Earth System Models. Nat. Commun. 11 (1), 522.
Fodor, N., Sándor, R., Orfanus, T., Lichner, L., Rajkai, K., 2011. Evaluation method dependency of measured saturated hydraulic conductivity. Geoderma 165 (1), 60–68.
Fuentes-Guevara, M.D., Armindo, R.A., Timm, L.C., Nemes, A., 2022. Data correlation structure controls pedotransfer function performance. J. Hydrol. 614, 128540.
Gao, H., Shao, M., 2015. Effects of temperature changes on soil hydraulic properties. Soil Tillage Res. 153, 145–154.
Gardner, W.R., 1958. Some steady-state solutoins of the unsaturated moisture flow equation with application to evaportation from a water table. Soil Sci. 85 (4), 228.
Garland, G., Koestel, J., Johannes, A., Heller, O., Doetterl, S., Or, D., Keller, T., 2024. Perspectives on the misconception of levitating soil aggregates. Soil 10 (1), 23–31.
Ghanbarian, B., Taslimitehrani, V., Dong, G., Pachepsky, Y.A., 2015. Sample dimensions effect on prediction of soil water retention curve and saturated hydraulic conductivity. J. Hydrol. 528, 127–137.
Gutmann, E.D., Small, E.E., 2007. A comparison of land surface model soil hydraulic properties estimated by inverse modeling and pedotransfer functions. Water Resour. Res. 43 (5).
Hardie, M.A., Doyle, R.B., Cotching, W.E., Mattern, K., Lisson, S., 2012. Influence of antecedent soil moisture on hydraulic conductivity in a series of texture-contrast soils. Hydrol. Process. 26 (20), 3079–3091.
Holthusen, D., Haas, C., Peth, S., Horn, R., 2012. Are standard values the best choice? a critical statement on rheological soil fluid properties viscosity and surface tension. Soil Tillage Res. 125, 61–71.
Iuss, 2022. World Reference Base for Soil Resources.: International soil classification system for naming soils and creating legends for soil maps, 4th ed. Vienna, Austria.
Jarvis, N.J., 2007. A review of non-equilibrium water flow and solute transport in soil macropores: principles, controlling factors and consequences for water quality. Eur. J. Soil Sci. 58 (3), 523–546.
Jirků, V., Kodešová, R., Nikodem, A., Mühlhanselová, M., Žigová, A., 2013. Temporal variability of structure and hydraulic properties of topsoil of three soil types. Geoderma 204–205, 43–58.
Jorda, H., Bechtold, M., Jarvis, N., Koestel, J., 2015. Using boosted regression trees to explore key factors controlling saturated and near-saturated hydraulic conductivity. Eur. J. Soil Sci. 66 (4), 744–756.
Kaiser, K., Guggenberger, G., 2003. Mineral surfaces and soil organic matter. Eur. J. Soil Sci. 54 (2), 219–236.
Kemper, W.D., Rosenau, R.C., 1986. Aggregate Stability and size distribution. In: Klute, A. (Ed.), Methods of Soil Analysis. SSSA Book Series. Soil Science Society of America, American Society of Agronomy, Madison, WI, USA, pp. 425–442.
Khodaverdiloo, H., Bahrami, A., Rahmati, M., Vereecken, H., Miryaghoubzadeh, M., Thompson, S., 2022. Recalibration of existing pedotransfer functions to estimate soil bulk density at a regional scale. Eur. J. Soil Sci. 73 (3).
Koestel, J., Fukumasu, J., Garland, G., Larsbo, M., Nimblad Svensson, D., 2021. Approaches to delineate aggregates in intact soil using X-ray imaging. Geoderma 402, 115360.
Kreiselmeier, J., Chandrasekhar, P., Weninger, T., Schwen, A., Julich, S., Feger, K.-H., Schwärzel, K., 2020. Temporal variations of the hydraulic conductivity characteristic under conventional and conservation tillage. Geoderma 362, 114127.
Levin, S.B., Briggs, M.A., Foks, S.S., Goodling, P.J., Raffensperger, J.P., Rosenberry, D.O., Scholl, M.A., Tiedeman, C.R., Webb, R.M., 2023. Uncertainties in measuring and estimating water-budget components: current state of the science. WIREs Water 10 (4).

Levy, G.J., Smith, H., Agassi, M., 1989. Water temperature effect on hydraulic conductivity and infiltration rate of soils. S. Afr. J. Plant Soil 6 (4), 240–244.
Li, Y., Chen, D., White, R.E., Zhu, A., Zhang, J., 2007. Estimating soil hydraulic properties of Fengqiu County soils in the North China Plain using pedo-transfer functions. Geoderma 138 (3–4), 261–271.
Lobe, I., Sandhage-Hofmann, A., Brodowski, S., Du Preez, C.C., Amelung, W., 2011. Aggregate dynamics and associated soil organic matter contents as influenced by prolonged arable cropping in the South African Highveld. Geoderma 162 (3–4), 251–259.
Matula, S., Miháliková, M., Lufinková, J., Báťková, K., 2015. The role of the initial soil water content in the determination of unsaturated soil hydraulic conductivity using a tension infiltrometer. Plant Soil Environ. 61 (11), 515–521.
Mohanty, B., 1998. Spatio-temporal dynamics of water and heat in a field soil. Soil Tillage Res. 47 (1–2), 133–143.
Nemes, A., Schaap, M.G., Wösten, J.H.M., 2003. Functional Evaluation of Pedotransfer Functions Derived from Different Scales of Data Collection. Soil Science Soc of Amer J 67 (4), 1093–1102.
Nemes, A., Wösten, J., Lilly, A., Oude Voshaar, J.H., 1999. Evaluation of different procedures to interpolate particle-size distributions to achieve compatibility within soil databases. Geoderma 90 (3–4), 187–202.
Pachepsky, Y., Park, Y., 2015. Saturated Hydraulic Conductivity of US Soils Grouped according to Textural Class and Bulk Density. Soil Science Soc of Amer J 79 (4), 1094–1100.
Popović, Z., Cerdà, A., 2023. Soil water repellency and plant cover: a state-of-knowledge review. Catena 229, 107213.
Pulido Moncada, M., Gabriels, D., Cornelis, W., Lobo, D., 2015. Comparing Aggregate Stability Tests for Soil Physical Quality Indicators. Land Degrad. Dev. 26 (8), 843–852.
Purushothaman, N.K., Reddy, N.N., Das, B.S., 2022. National-scale maps for soil aggregate size distribution parameters using pedotransfer functions and digital soil mapping data products. Geoderma 424, 116006.
R Core Team, 2025. R: a Language and Environment for Statistical Computing. R Foundation for Statistical Computing, Vienna, Austria.
Rabot, E., Wiesmeier, M., Schlüter, S., Vogel, H.-J., 2018. Soil structure as an indicator of soil functions: a review. Geoderma 314, 122–137.
Rahmati, M., Weihermüller, L., Vanderborght, J., Pachepsky, Y.A., Mao, L., Sadeghi, S. H., Moosavi, N., Kheirfam, H., Montzka, C., van Looy, K., Toth, B., Hazbavi, Z., Al Yamani, W., Albalasmeh, A.A., Alghzawi, M.Z., Angulo-Jaramillo, R., Antonino, A.C. D., Arampatzis, G., Armindo, R.A., Asadi, H., Bamutaze, Y., Batlle-Aguilar, J., Béchet, B., Becker, F., Blöschl, G., Bohne, K., Braud, I., Castellano, C., Cerdà, A., Chalhoub, M., Cichota, R., Císlerová, M., Clothier, B., Coquet, Y., Cornelis, W., Corradini, C., Coutinho, A.P., de Oliveira, M.B., de Macedo, J.R., Durães, M.F., Emami, H., Eskandari, I., Farajnia, A., Flammini, A., Fodor, N., Gharaibeh, M., Ghavimipanah, M.H., Ghezzehei, T.A., Giertz, S., Hatzigiannakis, E.G., Horn, R., Jiménez, J.J., Jacques, D., Keesstra, S.D., Kelishadi, H., Kiani-Harchegani, M., Kouselou, M., Kumar Jha, M., Lassabatere, L., Li, X., Liebig, M.A., Lichner, L., López, M.V., Machiwal, D., Mallants, D., Mallmann, M.S., de Oliveira Marques, J.D., Marshall, M.R., Mertens, J., Meunier, F., Mohammadi, M.H., Mohanty, B.P., Pulido-Moncada, M., Montenegro, S., Morbidelli, R., Moret-Fernández, D., Moosavi, A.A., Mosaddeghi, M.R., Mousavi, S.B., Mozaffari, H., Nabiollahi, K., Neyshabouri, M.R., Ottoni, M.V., Ottoni Filho, T.B., Pahlavan-Rad, M.R., Panagopoulos, A., Peth, S., Peyneau, P.-E., Picciafuoco, T., Poesen, J., Pulido, M., Reinert, D.J., Reinsch, S., Rezaei, M., Roberts, F.P., Robinson, D., Rodrigo-Comino, J., Rotunno Filho, O.C., Saito, T., Suganuma, H., Saltalippi, C., Sándor, R., Schütt, B., Seeger, M., Sepehrnia, N., Sharifi Moghaddam, E., Shukla, M., Shutaro, S., Sorando, R., Stanley, A.A., Strauss, P., Su, Z., Taghizadeh-Mehrjardi, R., Taguas, E., Teixeira, W. G., Vaezi, A.R., Vafakhah, M., Vogel, T., Vogeler, I., Votrubova, J., Werner, S., Winarski, T., Yilmaz, D., Young, M.H., Zacharias, S., Zeng, Y., Zhao, Y., Zhao, H., Vereecken, H., 2018. Development and analysis of the Soil Water Infiltration Global database. Earth Syst. Sci. Data 10 (3), 1237–1263.
Ren, J., Shen, Z., Yang, J., Zhao, J., Yin, J., 2014. Effects of Temperature and Dry Density on Hydraulic Conductivity of Silty Clay under Infiltration of Low-Temperature Water. Arab. J. Sci. Eng. 39 (1), 461–466.
Santanello, J.A., Peters-Lidard, C.D., Garcia, M.E., Mocko, D.M., Tischler, M.A., Moran, M.S., Thoma, D.P., 2007. Using remotely-sensed estimates of soil moisture to infer soil texture and hydraulic properties across a semi-arid watershed. Remote Sens. Environ. 110 (1), 79–97.
Sarkar, A., Maity, P.P., Ray, M., Chakraborty, D., Das, B., Bhatia, A., 2023. Inclusion of fractal dimension in four machine learning algorithms improves the prediction accuracy of mean weight diameter of soil. Eco. Inform. 74, 101959.
Schaap, M.G., Leij, F.J., 1998. Database-related accuracy and uncertainty of pedotransfer functions. Soil Sci. 163 (10), 765–779.
Schillaci, C., Acutis, M., Lombardo, L., Lipani, A., Fantappiè, M., Märker, M., Saia, S., 2017. Spatio-temporal topsoil organic carbon mapping of a semi-arid Mediterranean region: the role of land use, soil texture, topographic indices and the influence of remote sensing data to modelling. Sci. Total Environ. 601–602, 821–832.
Schoch, J., Nussbaum, M., Walthert, L., Carminati, A., Lehmann, P., 2025. Transferability of pedotransfer functions for estimating soil hydraulic properties: an analysis of controlling factors for forest soils in Switzerland. Geoderma 460, 117397.
Schoener, G., Stone, M.C., 2019. Impact of antecedent soil moisture on runoff from a semiarid catchment. J. Hydrol. 569, 627–636.
Schwärzel, K., Punzel, J., 2007. Hood Infiltrometer—A New Type of Tension Infiltrometer. Soil Science Soc of Amer J 71 (5), 1438–1447.
Shi, W., Zhang, Y., Weihermüller, L., Nemes, A., Schaap, M.G., Vereecken, H., 2026. Correlation of pedotransfer function residuals with input variables and the effect of database similarity on predictive performance. J. Hydrol. 671, 135192.
Shirazi, M.A., Boersma, L., 1984. A Unifying Quantitative Analysis of Soil Texture. Soil Science Soc of Amer J 48 (1), 142–147.
Six, J., Bossuyt, H., Degryze, S., Denef, K., 2004. A history of research on the link between (micro)aggregates, soil biota, and soil organic matter dynamics. Soil Tillage Res. 79 (1), 7–31.
Six, J., Elliott, E.T., Paustian, K., Doran, J.W., 1998. Aggregation and Soil Organic Matter Accumulation in Cultivated and Native Grassland Soils. Soil Science Soc of Amer J 62 (5), 1367–1377.
Szabó, B., Weynants, M., Weber, T.K.D., 2021. Updated European hydraulic pedotransfer functions with communicated uncertainties in the predicted variables (euptfv2). Geosci. Model Dev. 14 (1), 151–175.
Tóth, B., Weynants, M., Nemes, A., Makó, A., Bilas, G., Tóth, G., 2015. New generation of hydraulic pedotransfer functions for Europe. Eur. J. Soil Sci. 66 (1), 226–238.
Totsche, K.U., Amelung, W., Gerzabek, M.H., Guggenberger, G., Klumpp, E., Knief, C., Lehndorff, E., Mikutta, R., Peth, S., Prechtel, A., Ray, N., Kögel-Knabner, I., 2018. Microaggregates in Soils. z. Pflanzenernähr. Bodenk. 181 (1), 104–136.
Ugarte Nano, C.C., Nicolardot, B., Ubertosi, M., 2015. Near-saturated hydraulic conductivity measured on a swelling silty clay loam for three integrated weed management based cropping systems. Soil Tillage Res. 150, 192–200.
van Bavel, C.H.M., 1950. Mean Weight-Diameter of Soil Aggregates as a Statistical Index of Aggregation. Soil Science Soc of Amer J 14 (C), 20–23.
van Looy, K., Bouma, J., Herbst, M., Koestel, J., Minasny, B., Mishra, U., Montzka, C., Nemes, A., Pachepsky, Y.A., Padarian, J., Schaap, M.G., Tóth, B., Verhoef, A., Vanderborght, J., van der Ploeg, M.J., Weihermüller, L., Zacharias, S., Zhang, Y., Vereecken, H., 2017. Pedotransfer Functions in Earth System Science: challenges and Perspectives. Rev. Geophys. 55 (4), 1199–1256.
Vereecken, H., Amelung, W., Bauke, S.L., Bogena, H., Brüggemann, N., Montzka, C., Vanderborght, J., Bechtold, M., Blöschl, G., Carminati, A., Javaux, M., Konings, A.G., Kusche, J., Neuweiler, I., Or, D., Steele-Dunne, S., Verhoef, A., Young, M., Zhang, Y., 2022. Soil hydrology in the Earth system. Nat. Rev. Earth Environ. 3 (9), 573–587.
Vereecken, H., Maes, J., Feyen, J., 1990. Estimating unsaturated hydraulic conductivity from easily measured soil properties. Soil Sci. 149 (1), 1–12.
Vereecken, H., Weihermüller, L., Assouline, S., Šimůnek, J., Verhoef, A., Herbst, M., Archer, N., Mohanty, B., Montzka, C., Vanderborght, J., Balsamo, G., Bechtold, M., Boone, A., Chadburn, S., Cuntz, M., Decharme, B., Ducharne, A., Ek, M., Garrigues, S., Goergen, K., Ingwersen, J., Kollet, S., Lawrence, D.M., Li, Q., Or, D., Swenson, S., de Vrese, P., Walko, R., Wu, Y., Xue, Y., 2019. Infiltration from the Pedon to Global Grid Scales: an Overview and Outlook for Land Surface Modeling. Vadose Zone J. 18 (1), 1–53.
Vogel, H.-J., Balseiro-Romero, M., Kravchenko, A., Otten, W., Pot, V., Schlüter, S., Weller, U., Baveye, P.C., 2022. A holistic perspective on soil architecture is needed as a key to soil functions. Eur. J. Soil Sci. 73 (1).
Wang, Y., Shao, M., Liu, Z., 2012. Pedotransfer Functions for predicting Soil Hydraulic Properties of the Chinese Loess Plateau. Soil Sci. 177 (7), 424–432.
Wang, Z., Huang, L., Shao, M., 2024. Development of pedotransfer functions for predicting hydraulic parameters of van Genuchten model by incorporating environmental variables on the Qinghai-Tibet Plateau. Soil Tillage Res. 236, 105952.
Weynants, M., Montanarella, L., Toth, G., Arnoldussen, A., Anaya Romero, M., Bilas, G., Borresen, T., Cornelis, W., Daroussin, J., Da Gonçalves, M.C., Haugen, L.-E., Hennings, V., Houskova, B., Iovino, M., Javaux, M., Keay, C.A., Kätterer, T., Kvaerno, S., Laktinova, T., Lamorski, K., Lilly, A., Mako, A., Matula, S., Morari, F., Nemes, A., Patyka, N.V., Romano, N., Schindler, U., Shein, E., Slawinski, C., Strauss, P., Tóth, B., Woesten, H., 2013. European HYdropedological Data Inventory (EU-HYDI). EUR Scientific and Technical Research Series EUR 26053 EN (9789279323553).
Weynants, M., Vereecken, H., Javaux, M., 2009. Revisiting Vereecken Pedotransfer Functions: introducing a Closed-Form Hydraulic Model. Vadose Zone J. 8 (1), 86–95.
Wooding, R.A., 1968. Steady Infiltration from a Shallow Circular Pond. Water Resour. Res. 4 (6), 1259–1273.
Wösten, J., Lilly, A., Nemes, A., Le Bas, C., 1999. Development and use of a database of hydraulic properties of European soils. Geoderma 90 (3–4), 169–185.
Ye, L., Tan, W., Fang, L., Ji, L., Deng, H., 2018. Spatial analysis of soil aggregate stability in a small catchment of the Loess Plateau, China: I. Spatial Variability. Soil and Tillage Research 179, 71–81.
Zhang, Y., Schaap, M.G., 2019. Estimation of saturated hydraulic conductivity with pedotransfer functions: a review. J. Hydrol. 575, 1011–1030.
Zhou, X., Lin, H.S., White, E.A., 2008. Surface soil hydraulic properties in four soil series under different land uses and their temporal changes. Catena 73 (2), 180–188.